Doctoral Dissertation (Shinshu University)

Study of molecular size influences on processability and gelation of regenerated silk fibroin aqueous solution

March 2022

The Graduate School of Medicine, Science and Technology

Masaaki Aoki

Contents

Chapter 2. Fractionation of regenerated silk fibroin and characterization of the fractions

Chapter 3. Characterization of fabricated materials from fractions of regenerated silk fibroin

Chapter 4. Gelation mechanism of silk fibroin aqueous solution

Chapter 1.

General introduction

1.0. Composition of this dissertation

This dissertation is composed of 5 chapters (Figure 1-1). In chapter 1, the background and objectives of this study are summarized to clarify its significance. In chapter 2, it is described that the study of investigation of silk fibroin (SF) molecular weight (MW) fractionation using ammonium sulfate (AS) and properties of fractions. Chapter 3 describes the influence of SF MW on processability, morphology, structures and mechanical properties of materials fabricated from fractions which are prepared using AS fractionation as described in chapter 2. Chapter 4 shows the study of the relation between molecular size and gelation mechanism of SF aqueous solution. In chapter 5, this overall study is summarized and future perspectives are discussed.

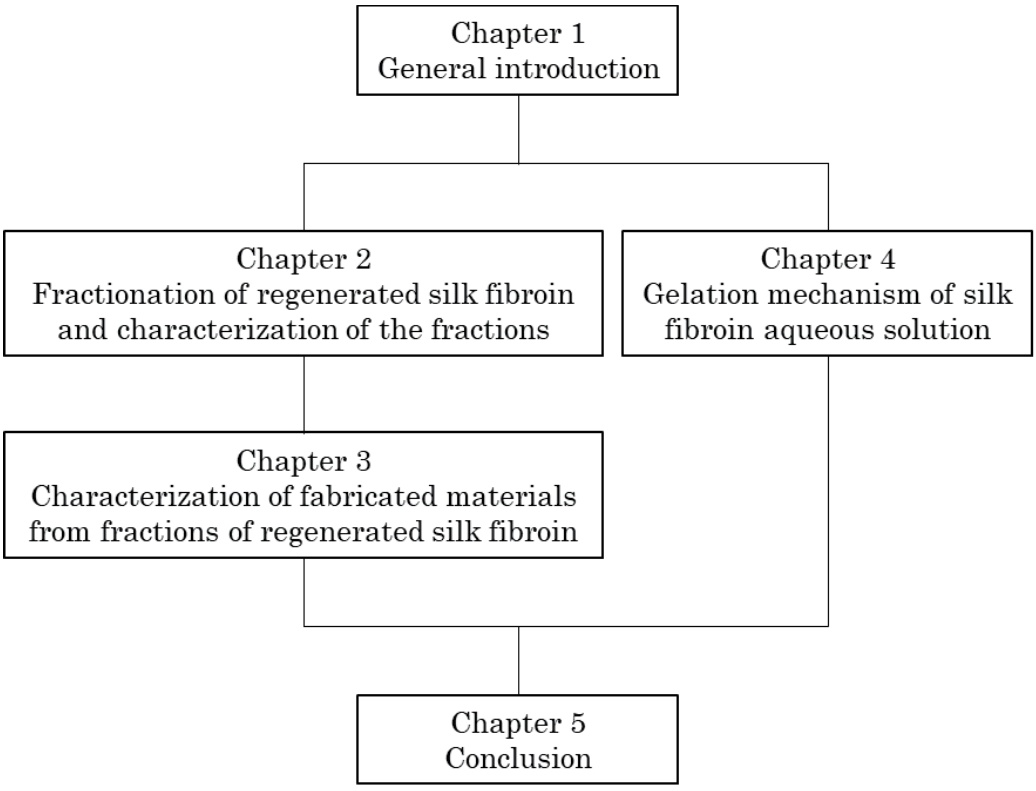

Figure 1-1. The composition of this doctoral dissertation.

1.1. Silk spun by domesticated silkworm

In general, silks are defined as protein polymers that are spun into fibers by some lepidoptera larvae [1–4]. The variety characteristics of silks are dependent on the specific source such as wild silkworm [5], spider [6], hornet [7] and bagworms [8].

Domesticated silkworm *Bombyx mori* has a high protein production capacity, and about 1500 m of silk can be obtained from a single silkworm cocoon [9]. Silk spun by silkworm is composed of two proteins, SF and sericin.

SF is synthesized in the posterior silk gland and stored in the middle silk gland (Figure 1-2). During storage in silk glands, the SF is concentrated and forms liquid crystal. At the beginning of spinning, SF flows through a narrow duct-like anterior silk gland, where shear stress induces crystal formation and orientation, and finally the silkworm shakes its head to draw SF from the spinneret and stretch SF to complete spinning [10]. Sericin is secreted in the middle silk gland and surrounded with SF [10].

It is known that silk has been used more than 5,000 years as material for clothing [11]. But not only in that field, SF has been investigated specifically for its application as a biomaterial in medicine, especially in the tissue engineering field, due to the biosafety which has exhibited during its extensive use for surgical sutures for many centuries [1]. In recent years, use of silk as medical materials has been focused increasingly.

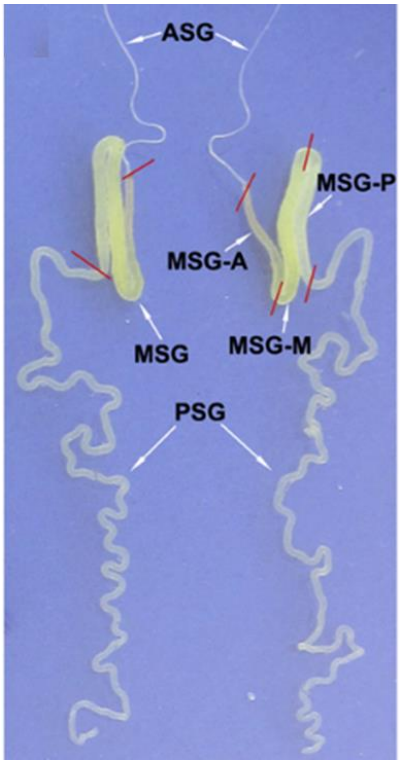

Figure 1-2. Silk glands of silkworm *Bombyx mori*. The silk gland is composed of anterior (ASG), middle (MSG), and posterior (PSG) regions. The MSG is divided into anterior (MSG-A), middle (MSG-M), and posterior (MSG-P) regions [12].

1.2. Structure of silk

Silk produced by the silkworm *Bombyx mori* consists of two types of proteins, fibroin and sericin, which are used to construct cocoons as the main frame fiber and glue, respectively [1] (Figure 1-3).

Sericin is a macromolecular protein with MW distribution of around 10-300 kDa and constitutes around 30% of silk protein [13]. Sericin is mainly composed of Ser, Asp, and Gly with ratio of around 30%, 15-20%, and 10-20%, respectively [14].

SF in silk glands has a heterodimer structure consisting of a H-chain protein and a L-chain protein bound by a disulfide bond. The H-chain protein

of SF has a characteristic amino acid sequence and is identified by a block copolymer with alternating in non-crystalline and crystalline regions block [15]. The non-crystalline region is conserved in the sequence of GTGSSGFGPYVA (X) GGYS (Z) GYEYAWSSESDFGT (X = Asn or His, Z = Arg, Ser, Asp, or a defect) [16]. The crystalline region also is consisted of a characteristic sequence, and generally a repeating sequence of GAGAGX (X = Ser or Tyr). The repeating structure of GAGAGX is known to promote the formation of ß-sheet structure, which contributes to the improvement of mechanical properties of SF.

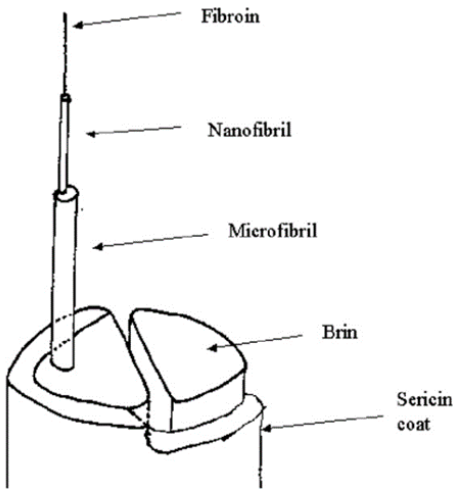

Figure 1-3. The structure of silk thread spun by *Bombyx mori* [17].

1.3. Silk as biomaterial

Many previous reports described that SF was a suitable substrate for the adhesion and proliferation of various cells and has found variety applications in the biomedical field, which can be attributed to its high tensile strength [18], predictable biodegradability [19], high oxygen permeability [18],

and low inflammatory characteristics [20]. Whereas, in the earlier studies using SF materials, it was reported that the inflammatory reactions in initial stages after implantation of SF materials [21]. However, the inflammatory response is a part of wound healing process and implantation of SF materials into living tissue induces wounding itself. The initial inflammatory response to SF materials *in vivo* is a normal wound healing and tissue regeneration process [22]. Based on the no severe inflammation in long period and the low inflammatory response *in vitro*, it is concluded that SF is a highly biocompatible material [22].

The sericin protein has been considered as a substance triggering inflammation and foreign body reactions because these reactions occurred when silk suture without enough degumming was used. However, the sericin layer contains a variety of substances [23], and they are more likely to induce biological reactions. Recently since it was shown that sericin combined with SF causes an inflammatory reaction, sericin should be removed by degumming through boiling in a weak alkali solution such as Na_2CO_3 before use for medical purposes [24].

1.4. Fabrication of SF

Although it was reported that silk fiber is an excellent textile material for practical use as a surgical scaffold in regenerative medicine [25], many studies have examined the fabrication of silk proteins beyond silk fibers to include films [26], gels [27], sponges [28], and nanofibers [29] adapted for medical use (Figure 1-4).

Figure 1-4. Materials fabricated from silk proteins.

1.4.1. Film

It has been known that polymers can fabricate to film form. SF is known to be available for film formed by casting or spin coating. SF film can be insolubilized through process using methanol [30] or heating [31], which induce the change of the SF structure from random coil to β-sheet and form the SF crystal [31]. Since medical materials contact with living organisms at its surface, it is important to elucidate the surface properties of the materials. Cell adhesion, cell proliferation, and synthetic substrates are dependent on the surface energy and surface charge of materials [32,33]. Liu et al. reported that SF film does not prevent the growth and biofunction of cells like fibroblasts, and concluded it has an excellent biocompatibility [34].

1.4.2. SF materials as scaffold for tissue engineering

Tissue engineering is a method of repairing and regenerating tissues and organs by combination of cells, growth factors and scaffolds [35]. In living tissue, cells generally grow on large network structure called extracellular matrix (ECM), which supports the cells as a scaffold [36] (Figure 1-5). When the tissue is damaged, and loss of cells and ECM occurs, the scaffold needs to be temporarily replaced by a scaffold material until the cells produce a new ECM. In this sense, scaffold materials are an essential part of tissue engineering. In recent years, there have been researching actively on cell scaffold materials in the field of regenerative medicine, such as bone [37,38], cartilage [39–41] and skin [42]. Kim et al. reported that porous structure and microfiber were suitable for cell scaffolds [43], and nanofiber and sponge are considered to satisfy these structures.

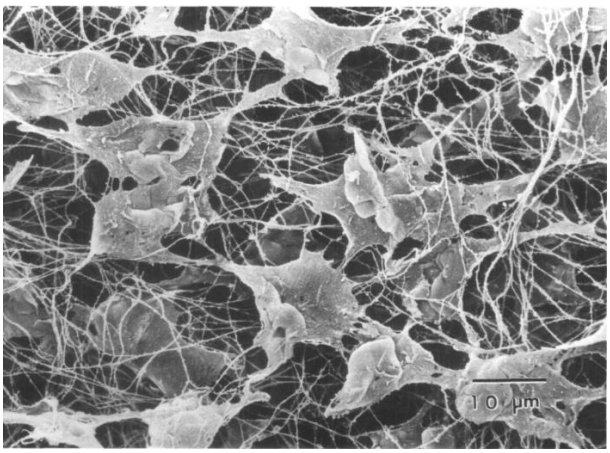

Figure 1-5. SEM image of the network of fibroblasts [36].

1.4.2.1. Nanofiber

As the diameter of polymer fiber material decreases from micrometers to nanometers, there appear some superior properties such as large surface area to volume ratio, flexibility in surface functionalities, and outstanding mechanical performance [44]. The polymer nanofibers with these amazing properties are expected to be optimal candidates for many applications.

Fabrication of nanofiber by self-assembly [45], phase separation [46], fused deposition modeling [47] and electrospinning [48] have been reported. Electrospinning is the methods for easily producing nanofiber by applying high voltage to polymer solution or molten polymer. In addition, electrospinning can be applied to many materials, and nanofiber fabrication of natural [44] or synthetic polymers and blending them [49] has been reported.

After the electrospinning of silk was first reported by Zarkoob, many reports can be found about fabrication of silk nanofiber by electrospinning. Sukigara et al. studied the effect of electrospinning parameters on the characteristics of the silk [50]. Electrospun SF fibers has the potential as cellular scaffolds in regenerative medicine [51]. Considering the nanofiber for medical applications, the use of the solvent with cytotoxicity or without biocompatibility should be avoided desirably such as HFIP (hexafluoro-2-propanol) and formic acid. The production of nanofiber nonwoven mats using electrospinning from a spinning solution containing a mixture of PEO and SF was reported [52], and even after washing nanofiber mats to remove away PEO, influence of the residual PEO on cell adhesion was reported by Jin et al.

[53]. Wang et al. has reported that SF fibers can be obtained from SF concentrated aqueous solution [54]. Recently, Kishimoto et al. reported that the fabrication of nanofiber nonwoven mat using electrospinning from only SF aqueous solution with low concentration is available [55]. Since these methods are not required organic solvent and have potential to control the fiber diameter and mechanical strength, expanding of application is expected.

1.4.2.2. Sponge

The fabrication of porous 3-D scaffolds (sponges) from regenerated silk fibroin (RSF) using HFIP was reported by Nazarov et al. [56]. It was reported that sponges prepared from SF dissolved in HFIP show lower biocompatibility than those prepared from aqueous-based SF [57]. This result suggested that using the sponges prepared from aqueous-based SF for tissue engineering is desirable. The freeze-thaw method to form of porous 3-D structure without freeze-drying, chemical cross-linking, or the aid of other polymeric materials was reported [58]. It was confirmed that the porous structures are formed in this method by crystallization of SF molecules in freezing state due to formation of ice crystal and concentration of SF molecules and solvent [59]. Hirakata et al. investigated using whole-area osteochondral defects of rabbit patella that healing effect of the SF sponge fabricated by freeze-thaw method, and it was indicated that the SF sponge covering has the potential to allow the early repair of large osteochondral defects [60]. The research in a wide range of fields is performed and further investigation is expected because of the specific properties of sponges.

1.4.2.3. Gel

Biopolymers such as polysaccharide and protein can form hydrogels, and galactomannan and collagen are well known as the example [61]. Attempts to use hydrogel for medical purposes have already been active for several decades [62].

Recently, injectable gel has been the subject of much research. The porous morphology is available to hold various drug molecules to be encapsulated in the gel matrix, and the encapsulated drugs can be subsequently released depending on the diffusion coefficient of the drug and the pore size of the gel network [63]. In addition, injectable gel has an advantage of invasive delivery to avoid the risk of surgical implantation or infection [64]. The study of injectable SF gel was reported for controlled and sustained delivery of insulin in diabetic animal model [65]. To control the gelation, elucidation of the gelation mechanism of RSF aqueous solution during storage requires some knowledge.

The Gelation of SF from an aqueous solution can be induced physically by application shear stress either with sonication [27,66] or vortexing [67], by temperature [68], by exposure to high pressure CO_2 [69], and chemically by lowering the pH [70] and by adding organic solvents such as methanol [71]. Whereas, it has been known that RSF in an aqueous solution is difficult to avoid the gelation during storage over a long period [72,73]. Usually, silk materials such as film, sponge, powder, gels, and non-woven mat, are fabricated from an aqueous solution, and the aqueous solution itself has already been used as an additive in cosmetics [73,74], daily products

[75], and foods [76]. Therefore, to produce a novel silk material, the stability of RSF aqueous solution must be secured for industrial applications.

1.5. Influence of polymer molecular size on the properties

Influence of molecular size including MW and its distribution on the mechanical, thermal, and rheological properties of polymer materials have been reported in previous studies [77,78]. The mechanical properties of regenerated cellulose fibers are affected positively by the increased MW of cellulose [79]. Reportedly, the tensile properties of cellulose fiber are strongly influenced by its MW distribution [80]. The thermal and rheological properties of polyethylene blends with bimodal MW distributions were elucidated by blending a high-MW polyethylene and low-MW polyethylene in different ratios [81]. The melting point and crystallization temperature were depended on MW and the MW distribution of blended polyethylene. The correlation between dynamic rheological properties and the MW distribution of blended polyethylene was confirmed. Further polymer surface properties were also affected by MW and its MW distribution. The molecules behavior of monodispersed and polydispersed polystyrene (PS) on the surface indicated that a surface of less than 30 kDa monodispersed PS film was more active than that of higher MW PS film and indicated that the surface of polydispersed PS film was less active than monodispersed PS film at a similar MW [82]. The MW distribution affected to the phase stability of a polymer mixture. A polymer blend of mixed polymers having a narrow MW distribution was reported giving phase stability compared to polymers with a

broad MW distribution [83]. Recently, it was described that the thermo-responsive transition of poly(N-isopropylacrylamide) was affected by MW and the distribution of MW [84]. Moreover, the MW and its distribution reflect to the processability of polymer materials for thermal and rheological properties of the polymer melt or solution [85].

1.6. SF molecular size

The studies focusing on molecular size of SF have been reported in previous studies. SF secreted into silk glands was originally a heterodimer protein consisting of H-chain and L-chain molecules with about 350 kDa and 26 kDa MW, respectively [86,87]. These molecular sizes of regenerated RSF decrease and disperse during degumming due to heat and alkaline hydrolysis, resulting in the reduction and distribution of MW [88] (Figure 1-6). In addition, the degummed SF is also dissolved in a solvent such as calcium nitrate/methanol [89], $CaCl_2/H_2O$/EtOH mixed solution [90], and LiBr aqueous solution [91] to prepare RSF solution. The dissolution process reportedly induces the cleavage of SF molecules [91]. Therefore, the RSF in the solution must be the cause of the MW reduction and MW distribution. Considering this characteristic of the appearance of decreased MW and MW distribution, and in order to develop the utilization technology of SF, the study focusing on molecular size is needed, but they have not been sufficiently investigated yet.

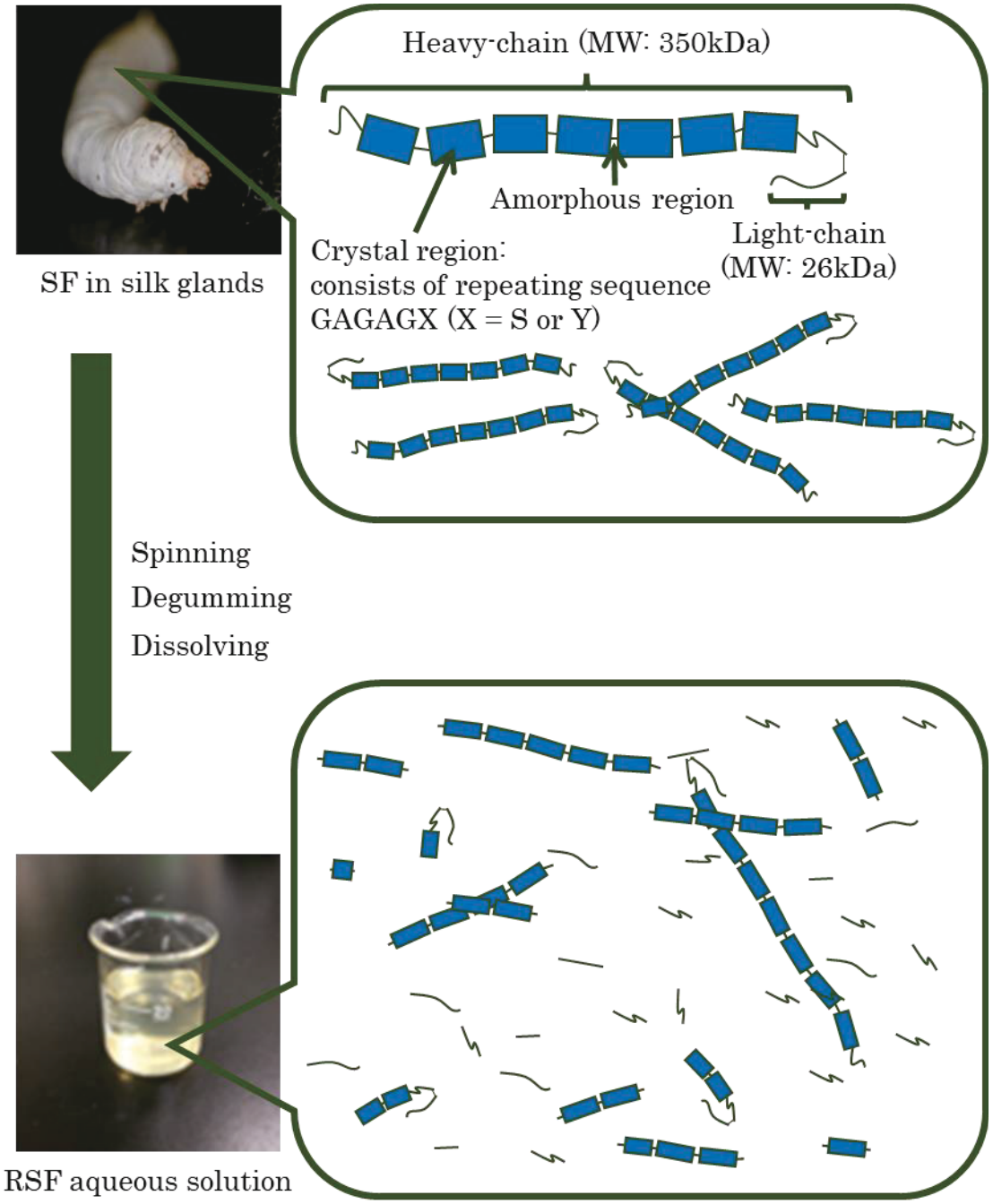

Figure 1-6. Change of SF MW through degumming and dissolving process.

1.7. The objective of this dissertation

The objective of this study is to elucidate the influence of the SF molecular size including MW and MW distribution on the properties of the

fabricated material and on the gelation of RSF aqueous solution. Firstly, appropriate conditions of MW fractionation using ammonium sulphate was investigated, and the properties of each fraction were examined. Furthermore, nanofiber and sponges were fabricated from the SF fractions aqueous solution to clarify the influence of molecular size on processability, and the structures and mechanical properties of the fabricated materials were evaluated. Secondly, the influence of molecular size on the gelation of aqueous RSF solution during storage was investigated in order to elucidate the gelation mechanism.

Chapter 2.

Fractionation of regenerated silk fibroin and characterization of the fractions

2.0. Introduction

It was previously reported that the effect of the molecular size on the properties of RSF aqueous solution with various degumming or dissolution conditions. Kishimoto et al. reported that the influence of SF molecular weight (MW) on viscosity of RSF aqueous solution [55]. Lee et al. has investigated effects of SF MW on conformation transition kinetics of RSF aqueous solution using circular dichroism spectroscopy [92]. However, since the decrease of MW was induced with heating or alkali in these studies, the existing MW and MW distribution in original RSF aqueous solution could not be investigated. Furthermore, the denaturation of SF may have been occurred by maintained conditions. To clarify the influence of the molecular size on the characteristics of original RSF aqueous solution, fractionation was attempted in this study.

Some methods for MW fractionation of proteins are well known, including gel permeation chromatography (GPC), ultrafiltration, and ultracentrifugation. Among them, ammonium sulfate (AS) precipitation is known as a rapid, mild inexpensive, and high-yield fractionation method [93]. The first investigation of the precipitation of proteins using salts including AS was reported more than a hundred years ago [94,95]. Recently, precipitation with AS was used for the study of the fractionation of equine antivenom IgG [96] and gelatin from big head carp [93]. AS precipitation was chosen to purify proteins in posterior silk glands to analyze the SF molecules [97], but no report has described the MW fractionation of RSF.

In this study, the objective was to elucidate the appropriate conditions

of fractionation of RSF by the AS precipitation process and the influences of the MW on the characteristics of SF. Firstly, the suitable conditions for RSF fractionation were investigated with various temperature and two methods. Then, each MW and molecular particle size of fractionated SFs was determined using GPC, polyacrylamide gel electrophoresis (SDS-PAGE), and dynamic light scattering (DLS). Amino acid composition and rheological property of the fractionated SFs were analyzed. Cast films of the fractionated SFs were fabricated and characterized by their secondary structure, surface properties, and cell proliferation.

2.1. Materials and methods

2.1.1. Preparation of RSF aqueous solution

Degummed silk thread (*Bombyx mori*, Shunrei-Shogetsu) was donated by Dr. Takabayashi (National Institute of Agrobiological Science, Okaya, Japan). The degummed silk thread was dissolved in 9 M LiBr (Fujifilm Wako Pure Chemical Corp., Tokyo, Japan) and was dialyzed for 3 days, with 6 times with reverse osmosis (RO) water to prepare an regenerated silk fibroin (RSF) aqueous solution with volume bath ratio 1 : 160. Then, the RSF aqueous solution was concentrated by air-drying at 25 °C as room temperature (r.t.) placed in the laboratory. The insoluble aggregations in the concentrated solution were removed by centrifugation (10,000 rpm × 30 min). The RSF aqueous solution concentration was measured by weight measurement after drying.

2.1.2. Fractionation of RSF

Fabrication of silk fibroin (SF) by AS precipitation was performed by two methods (1) AS powder addition (addition method (AM)) and (2) dialysis in AS solution (dialysis method (DM)) [98], respectively.

For the addition method (AM), RSF aqueous solution was adjusted to 1.5% (*w/v*) with RO water. The volume of RSF aqueous solution was adjusted to 100 mL with AS powder to become 7, 10, 15, and 20% of the saturated concentration. It was added gradually to the RSF aqueous solution under stirring for almost 30-60 min. After stirring was continued for 1 hr at r.t., the solution was incubated overnight at 4 °C or 37 °C. The precipitations at each AS saturated concentration were retrieved by centrifugation (10,000 rpm × 30 min). Then, the supernatant was used for fractionation at next phase continuously with a higher AS saturated concentration.

For the dialysis method (DM), RSF aqueous solution was adjusted to 1.5% (*w/v*) with RO water. After the volume of RSF aqueous solution was adjusted to 100 mL, it was placed in a dialysis membrane (MWCO: 12,000–14,000 Da; AS One Corp., Osaka, Japan). At first, the dialysis membrane was immersed into 500 mL of AS 7% saturation concentration solution. The dialysis solution was incubated overnight at 4 °C. The precipitate on the dialysis membrane was corrected by centrifugation (10,000 rpm × 30 min). Then the supernatant was placed in a new dialysis membrane for next fractionation. Furthermore, the supernatant solution in dialysis membrane was immersed into 10% AS saturated concentration solution and then the precipitate was collected. This fractionation process was carried out

repeatedly at 15 and 20% AS saturation concentration. The obtained precipitations of each fraction were washed using RO water and were freeze-dried for additional experiments, respectively. The fractionated SF materials are designated as 7SF-AM, 10SF-AM, 15SF-AM, and 20SF-AM, respectively, corresponding to the saturated concentration of AS for fractions 7%, 10%, 15%, and 20% and the SSF-AM for the fraction that is the retrieved supernatant for centrifugation of the 20% fraction. For designation of fractionation by the method DM, "DM" was added to each SF designation.

2.1.3. Fabrication of films

A film was formed by casting the 0.5% (*w/v*), 2 mL of fractionated SF aqueous solution onto a polystyrene dish (*Φ* 55 × 17; AS One Corp., Osaka, Japan), followed by incubation at 50 °C. The films were soaked into 80% (*v/v*) methanol for insolubilization and were incubated at 50 °C for drying.

The coated film was prepared by incubation of 0.5% (*w/v*) fractionated SF aqueous solution on a polyvinyl chloride plate at r.t. for 30 min. After the solution was removed, the coated film was incubated at 50 °C. The coated film was soaked into 80% (*v/v*) methanol for insolubilization and incubated at 50 °C.

2.1.4. Determination of MW of fractions

The fractionated SFs were dissolved in 9 M LiBr solution and were then dialyzed against RO water with bath ratio 1:160. The fractionated SF aqueous solutions were diluted to 0.1% (*w/v*) with an elution buffer (1/15 M

pH 7.0 phosphate buffer containing 2 M urea and 0.1 M Na_2SO_4) for measurement using gel permeation chromatography (GPC) analysis. I think this elution buffer did not affect significantly to MW determination, because the MW was comparatively evaluated with MW standard eluted by the same buffer. The sample solutions were filtered through a 0.45 μm hydrophilic PTFE membrane (Merck KGaA, Darmstadt, Germany) before measurement. GPC was performed using a high-performance liquid chromatograph (HPLC) system (Shimadzu Corp., Kyoto, Japan) with a GPC column (KW-804; Showa Denko K.K., Kanagawa, Japan) and HPLC was operated at a flow rate of 1.0 mL/min at 30 °C. Then the MW was estimated by calibration determined by using MW standard (Pullulan; Showa Denko K.K., Kanagawa, Japan). M_n, M_w and PDI were calculated using the following equations, respectively [99–101].

$$M_n = \Sigma\, H_i/\Sigma\, (H_i/M_i) \quad (1)$$

$$M_w = \Sigma\, (H_i \times M_i)/\Sigma\, H_i \quad (2)$$

$$\mathrm{PDI} = M_w/M_n \quad (3)$$

Therein, M_i stands for the MW of a molecule chain calculated by using Pullulan, H_i denotes the chromatogram heights, and i expresses a dividing point of retention.

SDS-PAGE was performed as follows. The fractionated SF aqueous solution in running buffer (Tris-HCl, SDS, sucrose, dithiothreitol (DTT) and bromophenol blue (BPB), E-T520L; ATTO Corp., Tokyo, Japan) were heated at 98 °C for 5 min and were then run on a 5–20 wt% polyacrylamide gradient

gel (E-T5520L; ATTO Corp., Tokyo, Japan). A molecular marker with range of 10–245 kDa (WSE-7020; ATTO Corp., Tokyo, Japan) was used for estimation of the MW and the distribution. Electrophoresis was carried out for 75 min with PageRun-R (ATTO Corp., Tokyo, Japan) using a current of 10.5 mA. After electrophoresis, the polyacrylamide gel was immersed in a stain solution (EzStain Aqua; ATTO Corp., Tokyo, Japan) and was then washed with RO water overnight.

2.1.5. Amino acid compositions analysis

After Hydrolysis of 0.01 g of freeze-dried fractionated SFs was performed in 6 M HCl_{aq} for 18 hr at 105 °C, the hydrolyzed solution was neutralized with 0.2 M sodium citrate and filtered through 0.45 μm filter (Hawach Scientific Co. Ltd., Shaanxi, China). The amino acid compositions were determined using a prominence amino acid analysis system (RF20AXS; Shimadzu Corp., Kyoto, Japan) and a Na-type amino acids mobile-phase kit (Shimadzu Corp., Kyoto, Japan). The amino acid compositions were glycine, alanine, serine, and tyrosine, which are the major amino acids in the SF molecule, and they were normalized using total concentration of serine and tyrosine and calculated.

2.1.6. Viscosity measurements

Measurement viscosity of the fractionated SF aqueous solution was performed at 20 °C using an oscillation type viscometer (VM-10A series, Viscomate; Sekonic Corp., Tokyo, Japan). The solution concentration was

adjusted to 0.5% (*w/v*) using RO water. Each sample was measured three times, and then the results were averaged.

2.1.7. RSF particle size distribution measurement

Particle size distribution measurement was performed by dynamic light scattering using nanoparticle measuring device (Zetasizer Nano ZS, Malvern, USA) with glass cell (AZLAB Glass Cell G-104, AS ONE, Osaka, Japan) at r.t.. The solution concentration was adjusted to 0.5% (*w/v*) using RO water. The measurements were repeated three times.

2.1.8. Water contact angle

Water contact angles of fractionated SF coated materials were measured using the sessile drop method with a contact angle meter (DMs-400; Kyowa Interface Science Co., Ltd., Saitama, Japan). After 2 μL of RO water was dropped onto the coated SF films, measurements were taken 60 times at intervals of 500 ms. The water contact angle data against time were extrapolated to 0 s; the angle at 0 s was defined as the water contact angle.

2.1.9. Zeta potential

The zeta potential for the films coated onto the glass were measured using a zeta potential and particle size analyzer (ELSZ-2000Z; Otsuka Electronics Co., Ltd., Osaka, Japan). For the measurement, the buffer was prepared as follows: 5 mM $NaCl_{aq}$ was added to adjust the concentration of phosphate buffer to 5 mM. Buffers of 3, 5, 7, and 9 pH were prepared with

HCl_{aq} and $NaOH_{aq}$. These buffer solutions were used to dilute the particle for monitoring, and the monitor dispersion for measurement was prepared.

2.1.10. FTIR

The measurement of FTIR was performed using an infrared spectrometer (Prestage-21; Shimadzu Corp., Kyoto, Japan) with ATR equipment (DuraSamplIR; Smiths Detection, London, UK) in the region of 600–4000 cm^{-1} at r.t. FTIR spectra were recorded with an accumulation of 30 scans and resolution of 4 cm^{-1}. The amide I (1600–1700 cm^{-1}) peaks of the FTIR spectra were decomposed and curve-fitted using software (OriginPro 8.1; OriginLab Corp., Northampton, MA, USA) for analysis of the secondary structures.

2.1.11. Cell culture

NIH3T3 cells were used for the test to evaluate the cell proliferation behavior on the coated films fabricated from fractionated SF. First, 5000 cells/mL/well were seeded on each coated sample and were incubated at 37 °C and 5% CO2. After 1, 3, 5, and 7 days of incubation, PBS rinsing, and addition of Triton X-100/PBS were performed such as the cell adhesion test described above for cell number counting on each culture day.

The cell number was determined by the LDH activity measurement method [102]. The measurement of LDH activity from cell lysate in Triton-×100/PBS solution was performed by NADH consumption using the change of the optical density at 340 nm. The cell number was calculated with

calibration data using LDH activity against the known cell number.

2.2. Results and Discussion

2.2.1. Influences of methods on SF fractionation

Figure 2-1 shows the GPC elution profiles of fractionated SF by the method direct addition of AS (AM, addition method) at 4 °C (A) and at 37 °C (B).

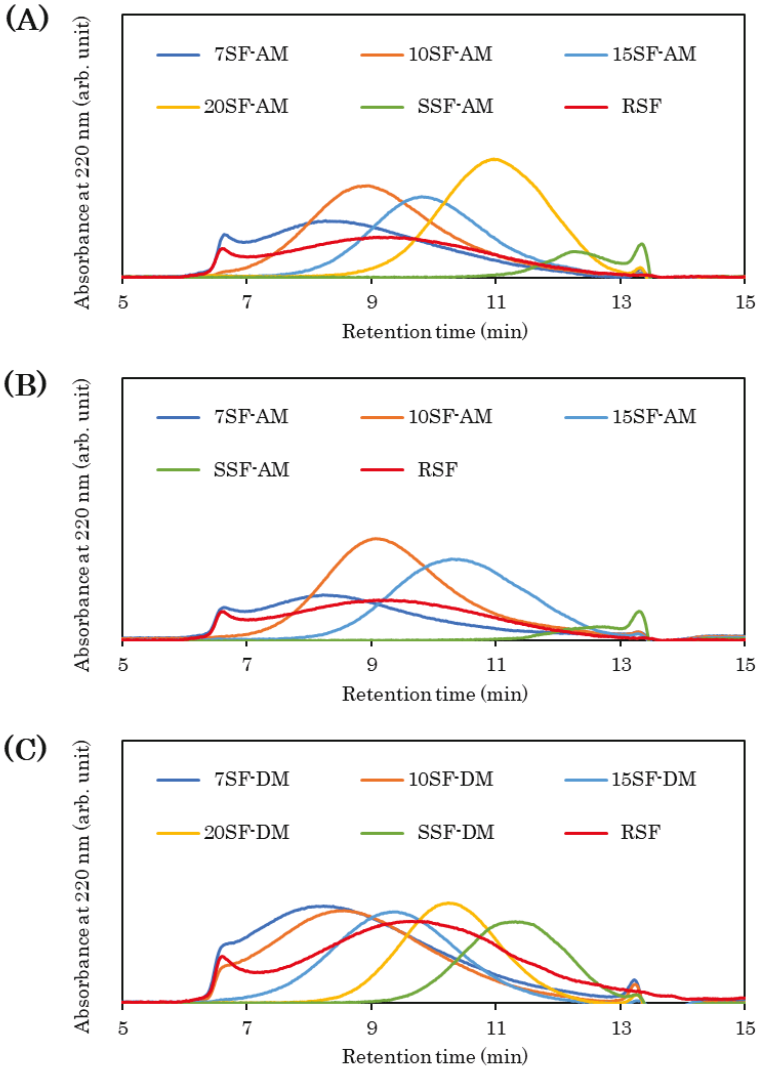

Figure 2-1. Elution profiles of GPC: (A) fractionated SFs by AM at 4 °C, (B) fractionated SFs by AM at 37 °C, (C) fractionated SFs by DM.

As the profiles show, the influence of temperature on the SF fractionation was observed. Although 20SF-AM was fractionated at 4 °C, this result was not obtained at 37 °C. Since the solubility of protein generally depends on the temperature, I inferred that the difference in fractionation profiles based on temperature derived from the protein solubility [103]. 20SF-AM might be difficult to precipitate at 37 °C because of its higher solubility than at lower temperature.

When AS powder was added directly to the RSF solution, avoiding a partially higher AS concentration portion in the solution against the expected AS concentration until complete dissolution was difficult. I used a dialysis method (DM) [98] for fractionation in which the RSF aqueous solution was placed in a dialysis membrane, with the tube immersed in the AS solution at each saturated concentration. Then the precipitate appearing in the dialysis membrane was collected by centrifugation, as described in the method section 2.1.2.. The GPC elution profile is presented in Figure 2-1 (C).

Fractionation was performed more clearly than that of the addition method (AM). The number-averaged molecular weight (M_n), weight-averaged molecular weight (M_w), polymer dispersion index (PDI), and yields of the respective fractionated SFs by both methods at 4 °C, which were calculated by calibration using MW standards pullulan (Figure 2-2), are presented in Table 2-1. When the two methods are compared, the MW (M_n and M_w) and PDI of every fractionated SF are similar. However, smaller deviation was observed at 7% and 10% fractionations on the DM than on AM. A higher concentration than the expected saturation concentration occurred partially

in the SF solution by direct addition of solid AS. At the high AS concentration, the lower MW SF fractions were precipitated. However, since the stable saturated concentration can be maintained through fractionation by the DM, the appropriate MW fractions of SF were precipitated at the saturated concentration with high reproducibility. As shown in Table 2-1, higher total yield was obtained with the DM than with the AM. Taken together, these results indicate that DM at 4 °C is suitable for RSF fractionation. The DM was used for further experiments in this study.

SDS-PAGE was used to analyze the MW and MW distributions of the fractionated SF for the respective saturated concentrations using DM. The SDS-PAGE profile indicates successful fractionation as shown Figure 2-3. The average MWs, which are the center of the smear band of each fractionated SF, were estimated as 245, 245, 100, 60, and 35 kDa, respectively, for 7SF-DM, 10SF-DM, 15SF-DM, 20SF-DM, and SSF-DM. The MWs estimated by SDS-PAGE were higher than those estimated by GPC because the MW standards used to estimate MW differed for SDS-PAGE and GPC, which were, respectively, protein and polysaccharide.

The amino acids that were specifically examined for the determination of the amino acid composition in each fractionated SF for this study were Gly, Ala, and Ser + Tyr. These amino acids were chosen as the most major and characteristic amino acids in the SF. The amounts of Gly and Ala were normalized with those of Ser + Tyr as 1; the ratio of the amino acid composition of each fractionated SF is shown in Table 2-2.

There was no significant difference of the amino acid composition

among 7SF-DM, 10SF-DM, and 15SF-DM. The ratios were similar to RSF, but a slightly higher content of Gly was found in 20SF-DM. It was known that SF has the unique repeated sequence (Gly-Ala-Gly-Ala-Gly-Ser/Tyr) in the H-chain of SF [104]. This sequence is known to form a crystal structure by the conformation of β-sheet [105–108]. Therefore, 7SF-DM, 10SF-DM, and 15SF-DM were expected to maintain the molecular structure of RSF, except for the MW.

The results of viscosity of fractionated SF aqueous solution were shown in Figure 2-4. This result indicated that the viscosity of the fractionated SF solution was dependent on its MW.

Figure 2-5 shows the result of SF particle size measured by DLS. 7SF-DM, 10SF-DM and RSF, which were included higher MW, showed broad particle size distribution, whereas 15SF-DM, 20SF-DM and SSF-DM, which contained mainly lower MW, had two peaks at almost 10 nm and 100 nm. It was found that SF MW affects to the particle size of SF in aqueous solution.

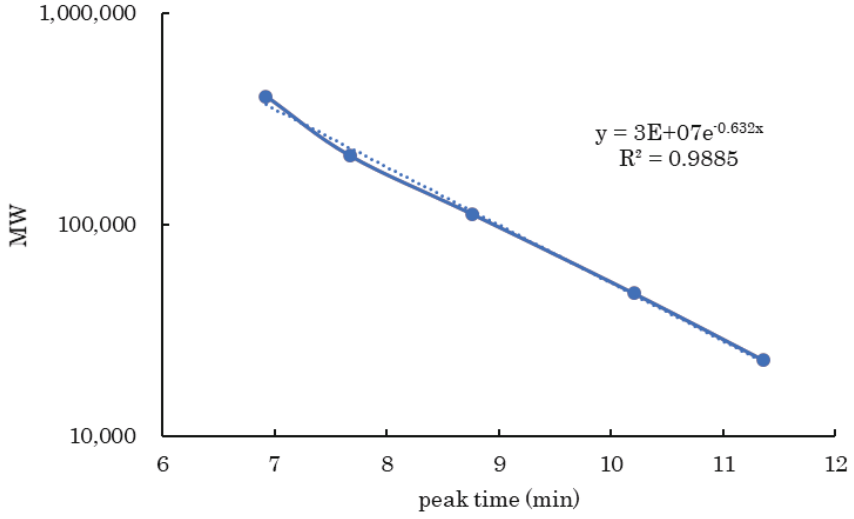

Figure 2-2. Calibration line using standard material Pullulan.

Table 2-1. Number-averaged molecular weight (M_n), weight-averaged molecular weight (M_w), polymer dispersion index (PDI) and ratios of precipitation yields at each fractionation. Fractionation was repeated three times: (A) AM and (B) DM.

(A)

Sample	M_n		M_w		PDI		Yield (%)	
	Avg.	Std.	Avg.	Std.	Avg.	Std.	Avg.	Std.
7SF-AM	75,000	9,600	190,000	20,000	2.5	0.44	17.0	8.1
10SF-AM	70,000	8,900	140,000	24,000	2.0	0.14	13.5	8.9
15SF-AM	46,000	4,400	76,000	8,100	1.7	0.10	8.16	8.6
20SF-AM	32,000	5,600	44,000	8,300	1.4	0.09	3.76	1.3
SSF-AM	15,000	6,000	19,000	8,700	1.2	0.08	0.98	0.56
RSF	52,000	1,500	140,000	12,000	2.6	0.29		
Total							43.4	13.9

(B)

Sample	M_n		M_w		PDI		Yield (%)	
	Avg.	Std.	Avg.	Std.	Avg.	Std.	Avg.	Std.
7SF-DM	66,000	2,900	160,000	11,000	2.3	0.13	15.8	2.0
10SF-DM	70,000	9,000	140,000	11,000	2.1	0.13	25.5	15.1
15SF-DM	51,000	11,000	82,000	15,000	1.6	0.14	11.1	3.7
20SF-DM	35,000	4,300	48,000	3,700	1.4	0.12	9.11	2.83
SSF-DM	17,000	4,500	21,000	6,400	1.2	0.06	1.66	0.63
RSF	54,000	9,100	130,000	15,000	2.4	0.14		
Total							67.7	16.5

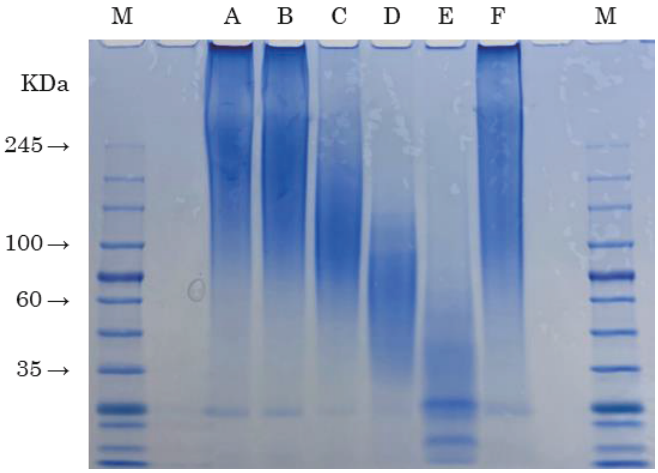

Figure 2-3. SDS-PAGE analysis of fractionated SFs by DM; Lane A, 7SF-DM; B, 10SF-DM; C, 15SF-DM; D, 20SF-DM; E, SSF-DM; F, RSF; and M, molecular weight marker.

Table 2-2. Ratio of amino acid composition of fractionated SF. The values of Gly and Ala were normalized by those of Ser + Tyr as 1.

	7SF-DM	10SF-DM	15SF-DM	20SF-DM	RSF
Gly	3.48	3.33	3.80	4.72	4.72
Ala	1.64	1.57	1.72	1.96	1.96
Ser + Tyr	1.00	1.00	1.00	1.00	1.00

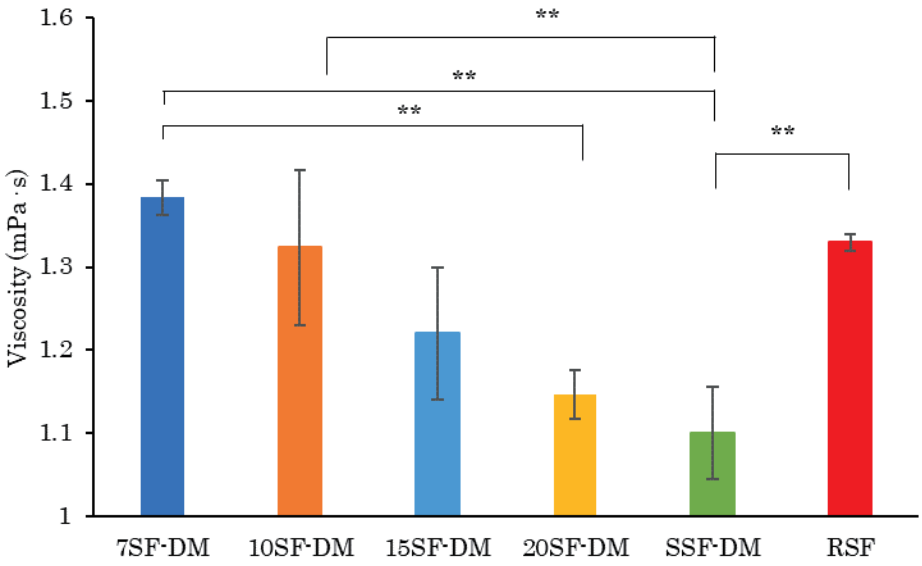

Figure 2-4. Viscosity of fractionated 0.5% (*w/v*) SF aqueous solution (** $p < 0.01$, * $p < 0.05$, $n = 3$ by Tukey–Kramer test).

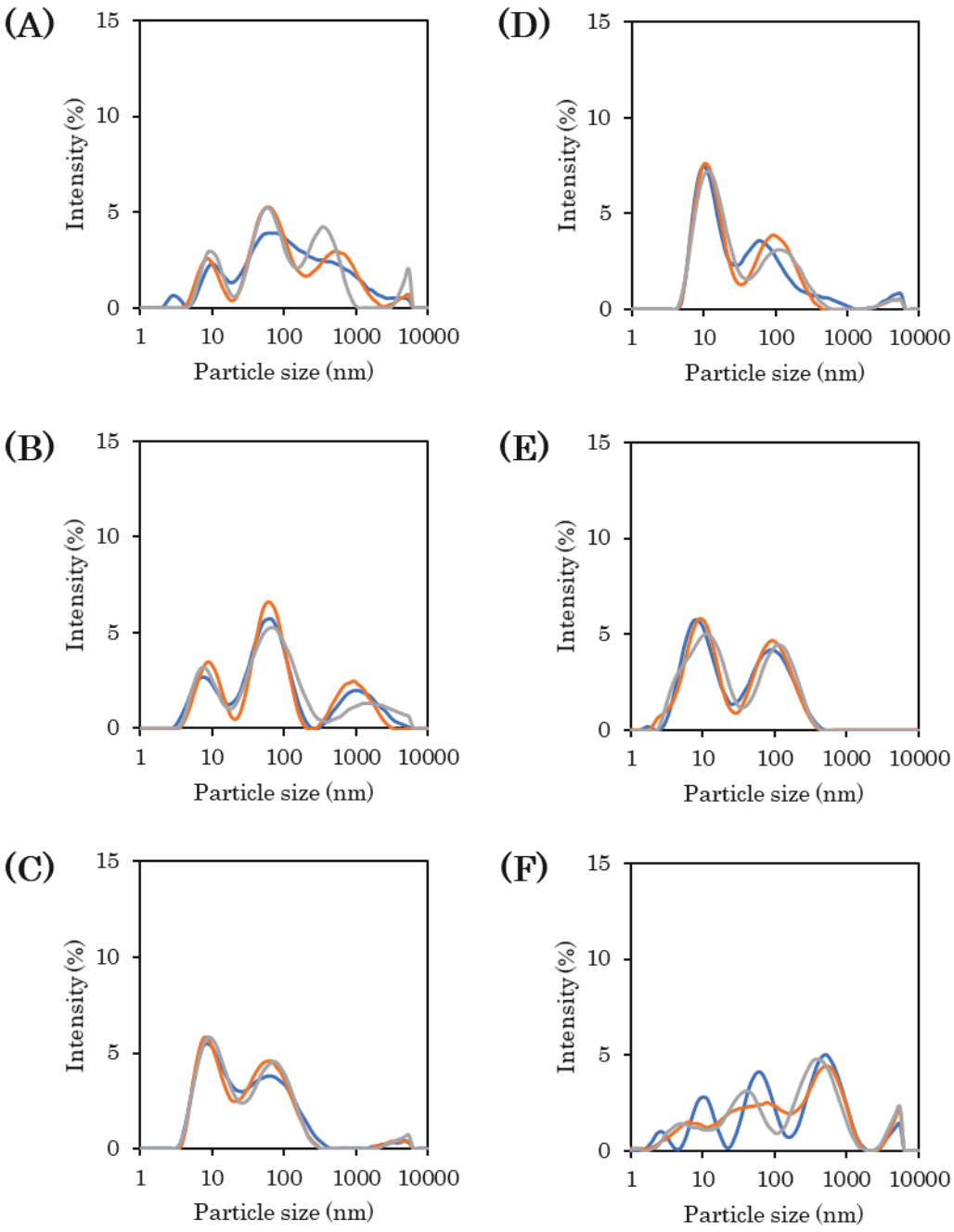

Figure 2-5. Particle size distribution in each fractionated SF aqueous solution. Figure shows 3 times measurements for each sample. (A): 7SF-DM, (B): 10SF-DM, (C): 15SF-DM, (D): 20SF-DM, (E): SSF-DM, (F): RSF.

2.2.2. Surface properties of films prepared from fractions

The measurement of water contact angle of the fractionated SF films was performed by coating SF onto the PVC substrate. The average water contact angles of 7SF-DM, 10SF-DM, 15SF-DM, 20SF-DM, and RSF were shown in Figure 2-6, respectively. There was no significant difference among the fractionated SF films and RSF films, except for 20SF-DM. A slightly higher contact angle of 20SF-DM might be explained by the amino acid composition of 20SF-DM, which has abundant hydrophobic amino acids Gly and Ala, as presented in Table 2-2. The dependence of MW on the water contact angle using coated films with different MW SF prepared by changing the degumming condition was reported [88]. The results showed the contact angle was lower for SF films with lower MW. The authors explained these results by the lower content of β-sheet in lower MW SF film. As described hereinafter, since there was no significant difference in β-sheet contents among the fractionated SFs, the higher contact angle of 20SF-DM film is inferred to derive from the abundant Gly and Ala in 20SF-DM.

Another surface property, the zeta potential of 20SF-DM film was measured and compared with the 7SF-DM and RSF film. Results obtained at pH 3, 5, 7, and 9 are shown in Figure 2-7. No clear influence of MW on the zeta potential was found. This result indicates that the ratio of charged amino acid of 20SF-DM is similar to that of RSF and the other fractionated SFs.

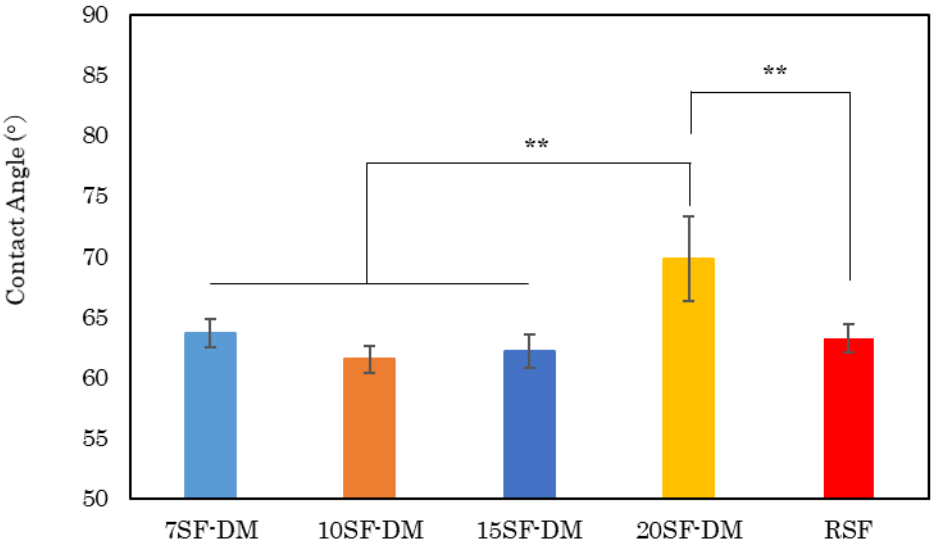

Figure 2-6. Water contact angle measurements of each SF fraction coated glass slides (** $p < 0.01$, $n = 4$ by Tukey–Kramer test).

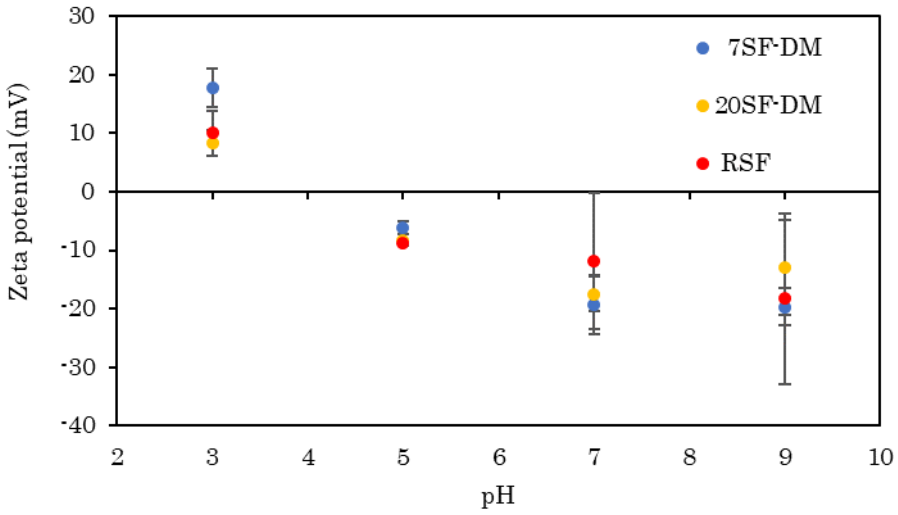

Figure 2-7. Zeta potential of coated films prepared from fractionated SF.

2.2.3. Secondary structure of films

The influence of MW on the structure of fractionated SF films was evaluated by ATR-FTIR measurements. Figure 2-8 shows the spectrum of as-cast (A) and methanol-treated (B) fractionated SF films at the region of amide I. No difference in spectra was found among the fractionated SF and RSF films as shown in Figure 2-8(A), (B). The amide I peak shows the reflection of the secondary structure of the protein. The peaks at 1640 cm^{-1} and 1620 cm^{-1} are attributed, respectively, to random and ß-sheet structures [109]. All fractionated SF films were able to change their structure to the ß-sheet structure by methanol treatment to make them insoluble, as is reported for SF films [110]. Figure 2-8 (C) shows the ß-sheet in the fractionated SFs films as-cast and after methanol treatment by estimation from the spectra [109]. There was no significant difference in the secondary structure of the cast films among fractionated SFs and RSFs. These results indicate that the MW of SF does not affect the structural formation in the fractionated SF film within the range of MW examined for this study.

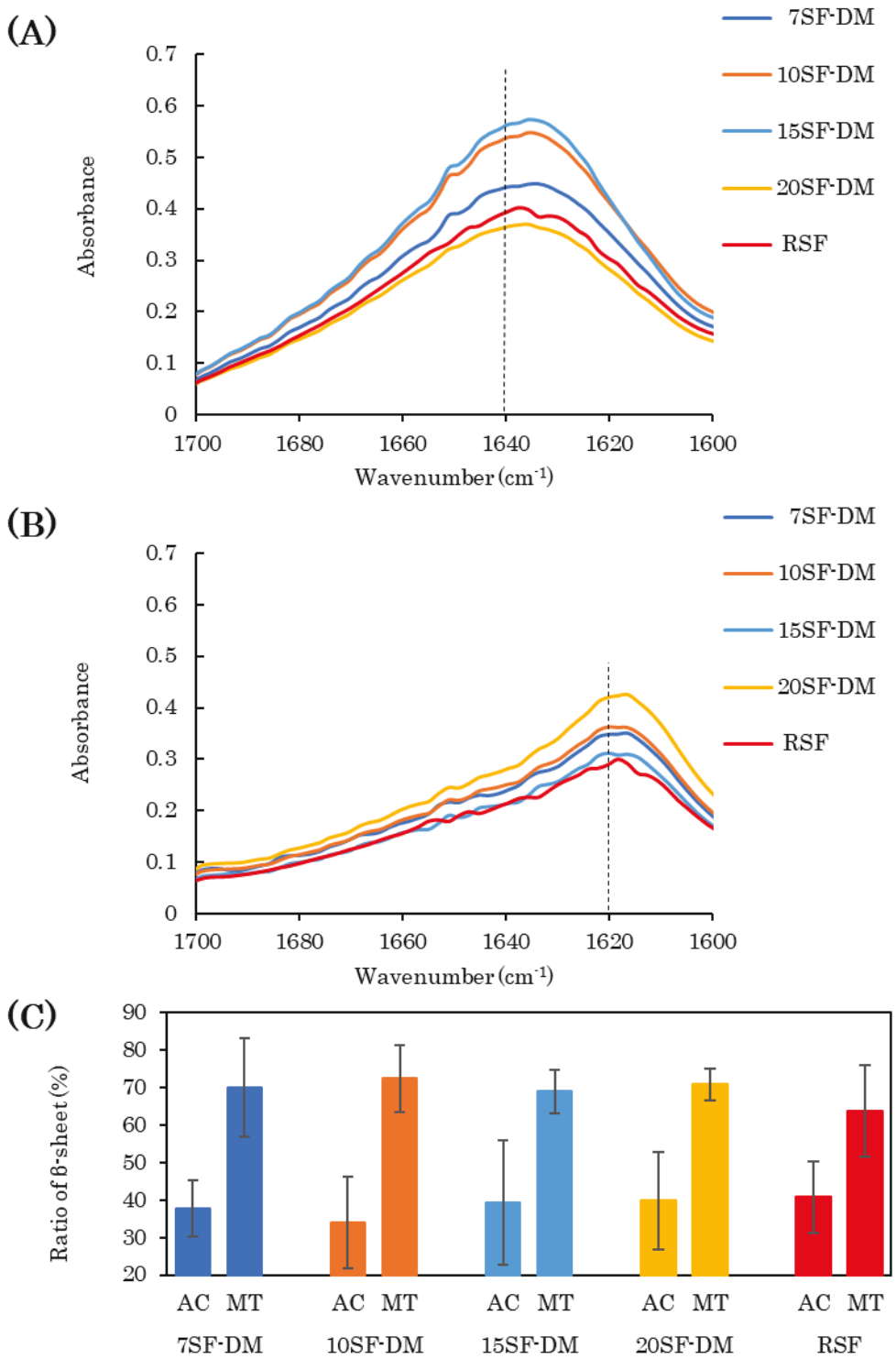

Figure 2-8. ATR-FTIR spectra at Amide I region in of fractionated SF films: (A) as-cast films and (B) films treated using methanol. Here, 1640 cm^{-1} and 1620 cm^{-1}, which are assigned for random structure and ß-sheets, are marked by dotted lines. (C): ß-sheet ratio for as-cast (AC) and methanol treatment (MT) films.

2.2.4. Cell proliferation test

In order to confirm the influence of MW on biocompatibility of SF, a cell proliferation test was performed on the coated film of the fractionated SFs. The cell proliferation curve is shown in Figure 2-9. Cells are able to proliferate on all fractionated SFs films. The doubling times calculated at the logarithmic phase of cell proliferation were 23.6, 26.1, 23.4, 23.3, 24.2, and 27.4 hr, respectively, on 7SF-DM, 10SF-DM, 15SF-DM, 20SF-DM, RSF, and TCPS. This result indicates no influence of SF MW on cell proliferation within the MW range in this study.

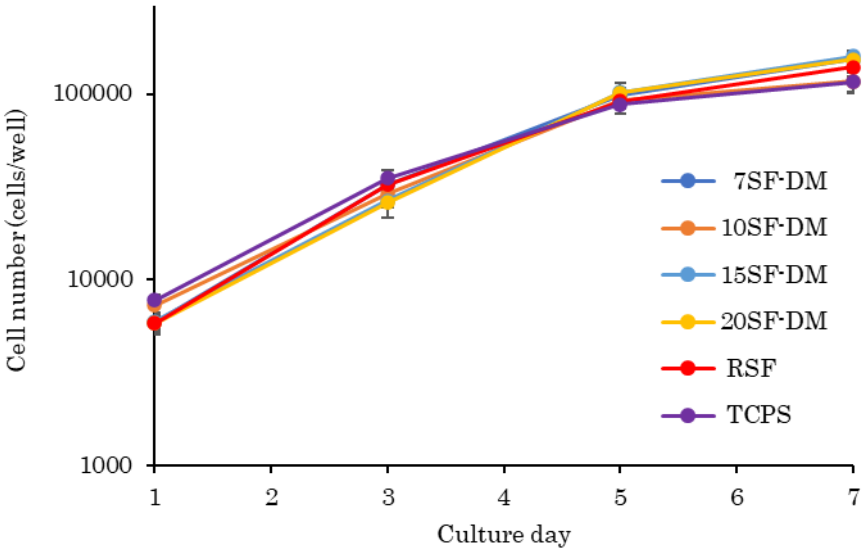

Figure 2-9. Proliferation of cell NIH3T3 on the coating film of the fractionated SFs and TCPS. The cell number is shown on a logarithmic scale.

2.3. Conclusion

Fractionation of SF from RSF aqueous solution was performed using

AS precipitation. Fractionation with AS using a dialysis membrane at low temperature was found to be the suitable fractionation method for SF. The fractionated SFs were characterized by GPC and SDS-PAGE, and the fractionated SFs showed different MW. The different distribution of SF molecular size in aqueous solution was found among fractions. The viscosity of each fractionated SF aqueous solution was depended on its MW. Amino acid analysis showed a different composition in the fractionation with lowest MW. Although the coated films formed from the fractionated SFs presented the same secondary structure, zeta potential, and cell proliferation, the lowest MW fractionated SF coated film had slightly greater hydrophobicity than the others. These results indicated that the MW difference of SF within the range of this study affects to some SF properties, but not to structures and cell proliferation.

Chapter 3.

Characterization of fabricated materials from fractions of regenerated silk fibroin

3.0. Introduction

Although many studies have been reported the fabrication of silk fibroin (SF) materials with various forms using regenerated silk fibroin (RSF) [111–113], few reports have described studies specifically examining the influence of molecular weight (MW) and its distribution on SF material properties and processability. For the fabrication of nanofiber nonwoven mats, the influence of MW on spinnability for electrospinning and the properties of SF electrospun from the aqueous solution [114] and formic acid solution [115] as the dope was investigated. The importance of MW for spinnability and the expression of properties such as mechanical strength and fiber diameter were clarified in those studies. Effect of MW of SF on spinnability of electrospinning and characteristics of electrospun SF fibers has been reported by some reports [114,116]. In those studies, the preparations of RSFs with different MW and MW distributions were performed by changing the degumming or dissolving conditions, such as time, temperature, and solvents, or alkaline hydrolysis of SF. However, these SFs are not strictly of the same origin, because of, mutually different preparation conditions, such as degumming and dissolving. Therefore, the possibility of changes in the structures and properties cannot be denied. To allay that concern, fractionation of MW-dispersed SF can be an appropriate method to obtain SFs with different MW and MW distributions, despite having the same origin.

The objective was to elucidate the effects of MW on SF fabrication in this study. The fractionation using ammonium sulfate was performed for fabrication materials. A nanofiber nonwoven mat and 3D porous sponge were

fabricated from the fractionated SF aqueous solution. Then their morphology were found by SEM, and they are analyzed to elucidate the structures and mechanical properties.

3.1. Materials and methods

3.1.1. Preparation of RSF aqueous solution

Bombyx mori cocoons were obtained from Art Co. Ltd., Gunma, Japan. For degumming, chrysalises were removed from the cocoons, and the cocoon layers were cut into 5 mm squares with scissors. The cut cocoon layers were immersed in 0.02 M Na_2CO_3 solution heated at 95 °C with bath ratio of 1:150, and stirred for 30 minutes. The degummed silk was washed with RO water and dried at 60 °C overnight. After degumming and drying, RSF aqueous solution was prepared thorough dissolution and dialysis process with the same method as section 2.1.1..

3.1.2. SF fractionation for fabrication of materials

The fractionation for fabrication of materials was performed with same method as section 2.1.2. except number of fractionation for each AS concentration. Since large amounts of SFs are required for fabrication of the SF materials, I selected two AS saturated concentrations for the fractionation of SF to obtain the SFs of different MWs: 7 and 20%, designated, respectively, as 7SF-DM2 and 20SF-DM2.

3.1.3. Fabrication of SF materials

The SF nanofiber nonwoven mat was fabricated by electrospinning. The electrospinning was performed using a solution type electrospinning system (Nanon-3; MECC Co., Ltd., Fukuoka, Japan) as following conditions. The concentration of fractionated SF aqueous solution was adjusted to 8% (*w/v*) with RO water and pH to 10.5 with 5 M NaOH (Fujifilm Wako Pure Chemical Corp., Tokyo, Japan) with ethanol added (99.5% (*v/v*); Fujifilm Wako Pure Chemical Corp., Tokyo, Japan) to 3% (*v/v*) concentration, then stirred at r.t. Electrospinning was performed at 18 kV with a distance of 20 cm between the spinneret and collector. The electrospun nonwoven mat was incubated in water vapor under 37 °C for 30 min to be insolubilized.

3D porous structures (sponges) were fabricated by freeze–thaw processing according to processes described in previous report [117]. The SF aqueous solution concentration was diluted to 2% (*w/v*) and 4% (*w/v*) with RO water; DMSO (Fujifilm Wako Pure Chemical Corp., Tokyo, Japan) was mixed at 1% (*v/v*) concentration. The solution was placed in an aluminum mold and frozen to −20 °C under programmed control, and then it was thawed at r.t.

3.1.4. Secondary structure

The FTIR spectra were measured, and the amide I (1600–1700 cm^{-1}) peaks of the FTIR spectra were decomposed and curve-fitted for analysis of the β-sheet content with same method as section 2.1.10..

The crystallinity index of the fractionated SF nanofiber nonwoven mat was calculated from the amide III band in the FTIR spectrum by previously

reported method [116]. The crystallinity index was calculated using following equation:

$$\text{Crystallinity index (\%)} = \text{Absorbance at 1260 cm}^{-1}/\text{Absorbance at 1235 cm}^{-1} \times 100$$

3.1.5. Mechanical tests

To evaluate mechanical properties, tensile tests for the fractionated SF nanofiber nonwoven mats were performed using a test machine (EZ-SX; Shimadzu Corp., Kyoto, Japan) with a 5 N load cell. The sample length was adjusted to 30 mm. The crosshead speed was set to 10 mm/min. A micrometer (Digimatic micrometer MDQ-30MX; Mitsutoyo Corp., Kanagawa, Japan) was used for the measurement of sample thickness. Measurement was performed at several points, and the averaged and cross-sectional areas were calculated. The measurement of compression modulus of fractionated SF sponges was performed using a test apparatus (EZ Test EZ-S; Shimadzu Corp., Kyoto, Japan) with a 50 N load cell at 5 mm/min of compression speed. The compression modulus determined by calculation from the average of 10 highest slope in the stress–strain curve.

3.1.6. Scanning electron microscopy (SEM)

After coating with platinum on the SF samples, scanning electron microscope images were taken at 10 kV (SEM: JSM-6010LA; JEOL Ltd., Tokyo, Japan). The fiber diameter of nanofiber and the diameter of the pore size of sponges were determined using software (ImageJ NIH, 1.53e) from

SEM images.

3.2. Results and Discussion

3.2.1. Fabrication of fractionated SFs

The peak MWs of 7SF-DM2 and 20SF-DM2 were estimated from the GPC profiles of the fractionated SFs shown in Figure 3-1, respectively, as 150,000 and 85,000. They are well-separated higher and lower than RSF with 120,000 of peak MW. The viscosity of aqueous solution of each fraction at 8.0% (*w/v*) concentration was the following: 18.3 ± 0.5, 14.3 ± 1.4, and 16.9 ± 0.6 mPa · s, respectively, for 7SF-DM2, 20SF-DM2, and RSF.

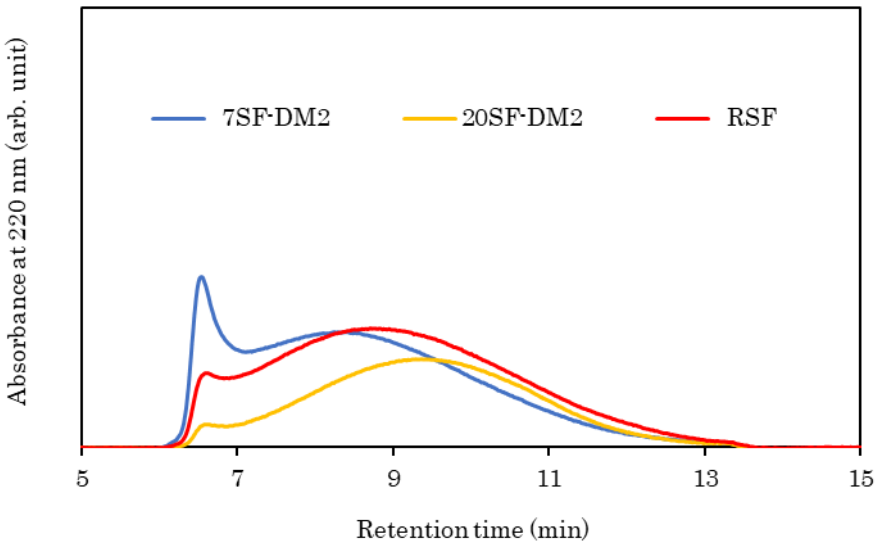

Figure 3-1. GPC elution profiles of SFs fractionated by DM with 7 % and 20% of saturated concentration AS and NSF.

3.2.2. Nanofiber nonwoven mat

In one report, SF nanofiber nonwoven mats prepared from all aqueous

RSF solution as spinning solution by the electrospinning process was described [118]. Both fractionated SF aqueous solution, 7SF-DM2 and 20SF-DM2 were available to be used for a nanofiber mat by electrospinning, similarly to RSF. The morphologies of nanofiber observed by SEM are shown in Figure 3-2. There was not significant difference of fiber diameters among SFs and RSF, and the diameter was estimated at around 400 nm. The fiber morphology of the 7SF-DM2 nonwoven mat was the same as that of RSF, but several beads appeared on the fibers of 20SF-DM2 nonwoven mat. It was reported by Kishimoto et al. that beads were induced in the electrospun SF nonwoven mat by lower MW SF [114]. The β-sheet contents and the crystallinity index among the fractionated SFs and RSF nanofibers determined by ATR-FTIR spectrum (Figure 3-3) were observed, and no significant difference was found. These results are in good agreement with the fractionation results of, as described section 2.2.3. The mechanical properties of the fractionated SF nanofiber nonwoven mat measured in the tensile test and, according to the strain–stress curve (A), and the breaking strain (B), breaking stress (C), and Young's modulus (D) are shown in Figure 3-4. The Young's modulus of the 20SF-DM2 nanofiber was the same as that of the 7SF-DM2 and RSF nanofiber, but the breaking stress and strain of the 20SF-DM2 nanofiber were significantly lower. This finding is in good agreement with results reported [85] for the dependence of MW on the mechanical properties of SF nanofibers. The strain at breaking of the 7SF-DM2 nanofiber was much higher than that of 20SF-DM2 and even of the RSF nanofiber. These results show that the toughness of 7SF-DM2 nanofiber is

superior to that of RSF nanofibers. These results indicate that the MW of SF is an important factor in the fabrication by electrospinning and an important factor affecting the mechanical properties of the resulting nanofiber nonwoven mat.

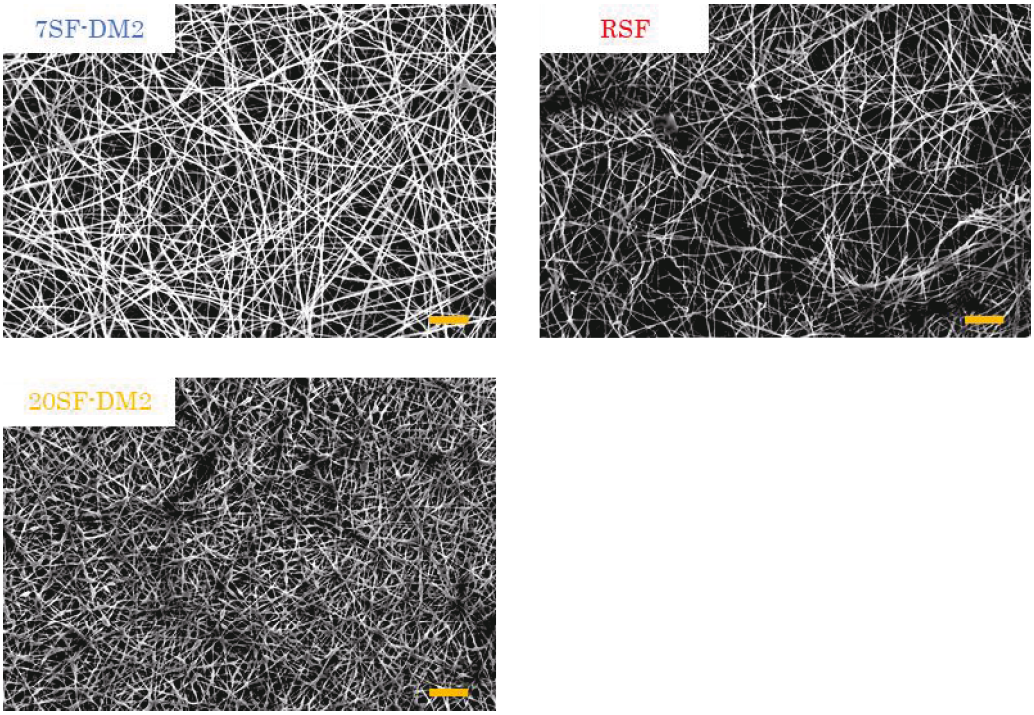

Figure 3-2. SEM images of nanofiber nonwoven mat using electrospinning from fractionated SF. Scale bar = 10 μm.

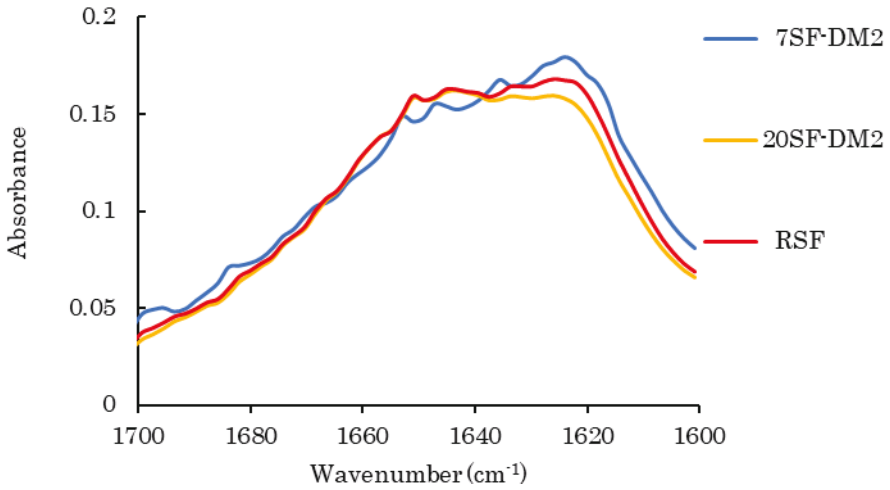

Figure 3-3. ATR-FTIR spectra at amide I region in of electrospun nanofiber nonwoven mat from fractionated SF.

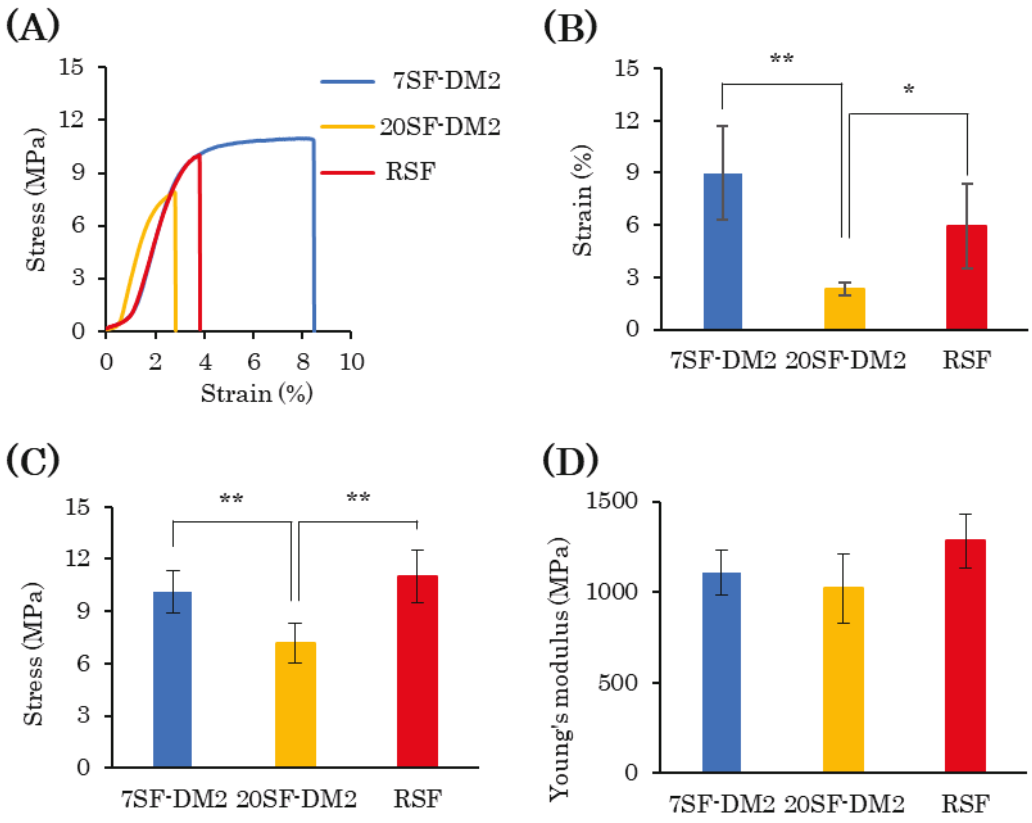

Figure 3-4. Tensile tests of SF nanofiber nonwoven mat fabricated using electrospinning from fractionated SF aqueous solution: (A) Typical stress–strain curve; (B) Influence of MW of SFs on strain at breaking (** $p < 0.01$, * $p < 0.05$, $n = 5$ by Tukey–Kramer test); (C) Influence of MW of SFs on stress at breaking (** $p < 0.01$, $n = 5$ by Tukey–Kramer test); (D) Influence of MW on Young's modulus. No significant differences among fractions and RSF were found by Tukey–Kramer test ($n = 5$, $p > 0.05$).

3.2.3. Porous 3D structure (sponge)

The porous 3D structure (sponge) of SF is available to be fabricated by freeze–thaw processing using RSF aqueous solution mixed with a small amount of water-miscible organic solvent such as DMSO [117]. Both fractionated SF aqueous solutions could be used for the fabrication of SF sponges by freeze–thaw processing. As shown in Figure 3-5, the pore

structure was observed by SEM. There was not apparent difference of the pore shape between the fractionated SFs and RSF. Figure 3-6 show the average pore size as measured using SEM images. The pore size of the 7SF-DM2 sponge was found to be markedly larger than those of the 20SF-DM2 sponge. I inferred that the pores of the 20SF-DM2 sponge became smaller than those of 7SF-DM2, as follows. The pore size of the SF sponge fabricated by the freeze–thaw process is determined by the size of the ice crystals grown during the freezing time. The slower the dissipation of the ice crystallization heat, the larger the ice crystals can grow. The SF molecules with lower MW can dissolve at a higher concentration in the aqueous solution than the higher MW fraction SF molecules. Since the specific heat capacity of the aqueous solution is lower at a higher solute concentration, the heat of ice crystallization in the lower MW fractionated SF solution can escape more faster than in the higher MW fractionated SF solution. The RSF sponge pore sizes were observed between 7SF-DM2 and 20SF-DM2. These results indicate that the MW of the fractionated SF affects the pore size of SF sponge, but the influence was small.

The ATR-FTIR spectra of the SF sponges fabricated from the fraction were measured, and Similar spectra with a peak at 1625 cm^{-1} were obtained as shown in Figure 3-7. The content of ß-sheet structure was estimated at around 61–65% of 2% (*w/v*) and as around 65–66% of 4% (*w/v*) fractionated SF sponges. The MW did not affect the secondary structure of the fractionated SF sponge as the film and nanofiber did.

The compressive modulus of the fractionated SFs sponges is shown in

Table 3-1. There was no significant difference among the SFs and RSF sponges at 2% concentration, but at 4% sponge, the 20SF-DM2 sponge showed a markedly higher compressive modulus than the others. As shown in Figure 3-6, I inferred that the higher compressive modulus of the 4% 20SF-DM2 sponge might derive from the smaller pore size. For the 2% sponge, since the SF content in the sponge wall is too small to detect the mechanical difference, the apparent compressive modulus of 20SF-DM2 sponge might be measured similarly to that of the 7SF-DM2 sponge.

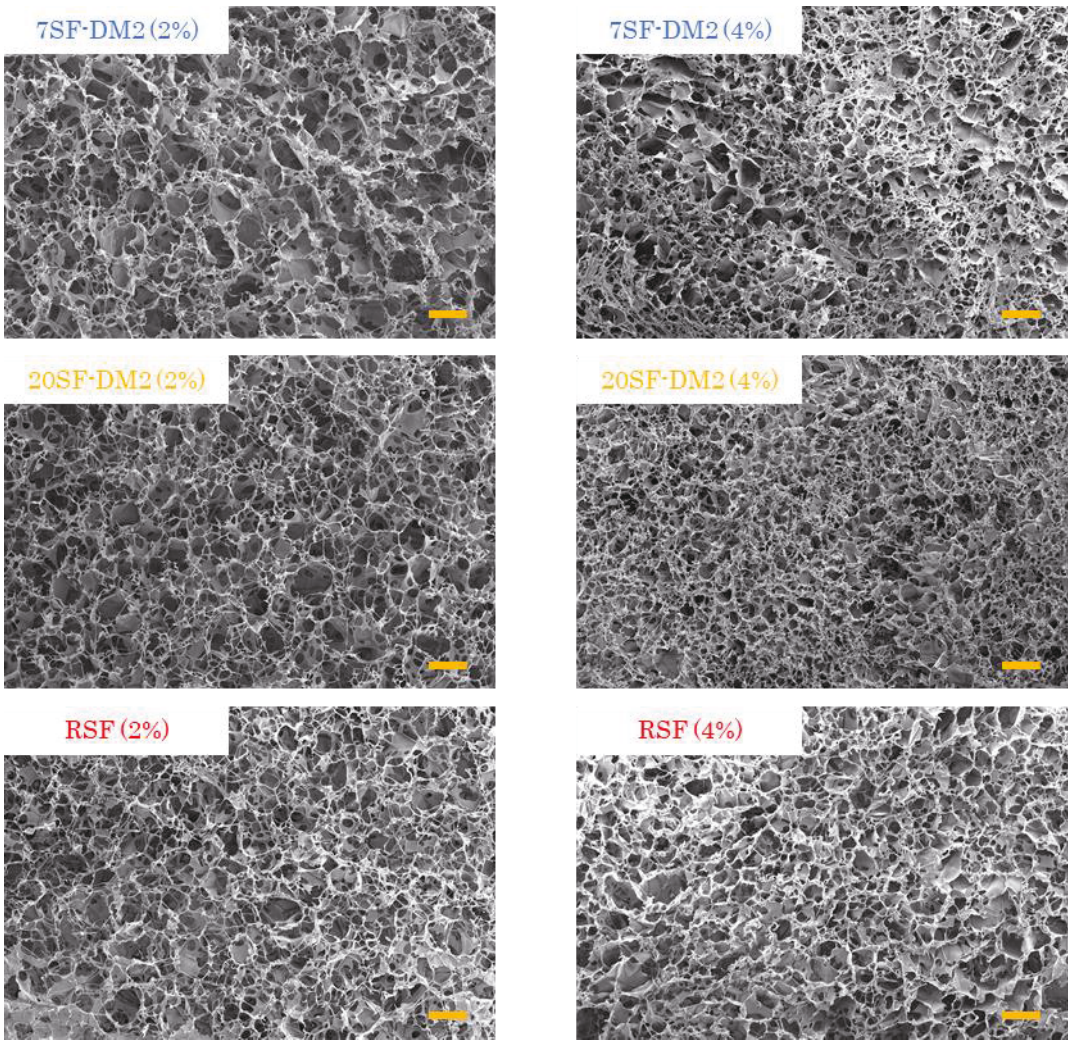

Figure 3-5. SEM images of sponges fabricated from the fractionated SFs by freeze-thawing. Scale bar = 100 μm.

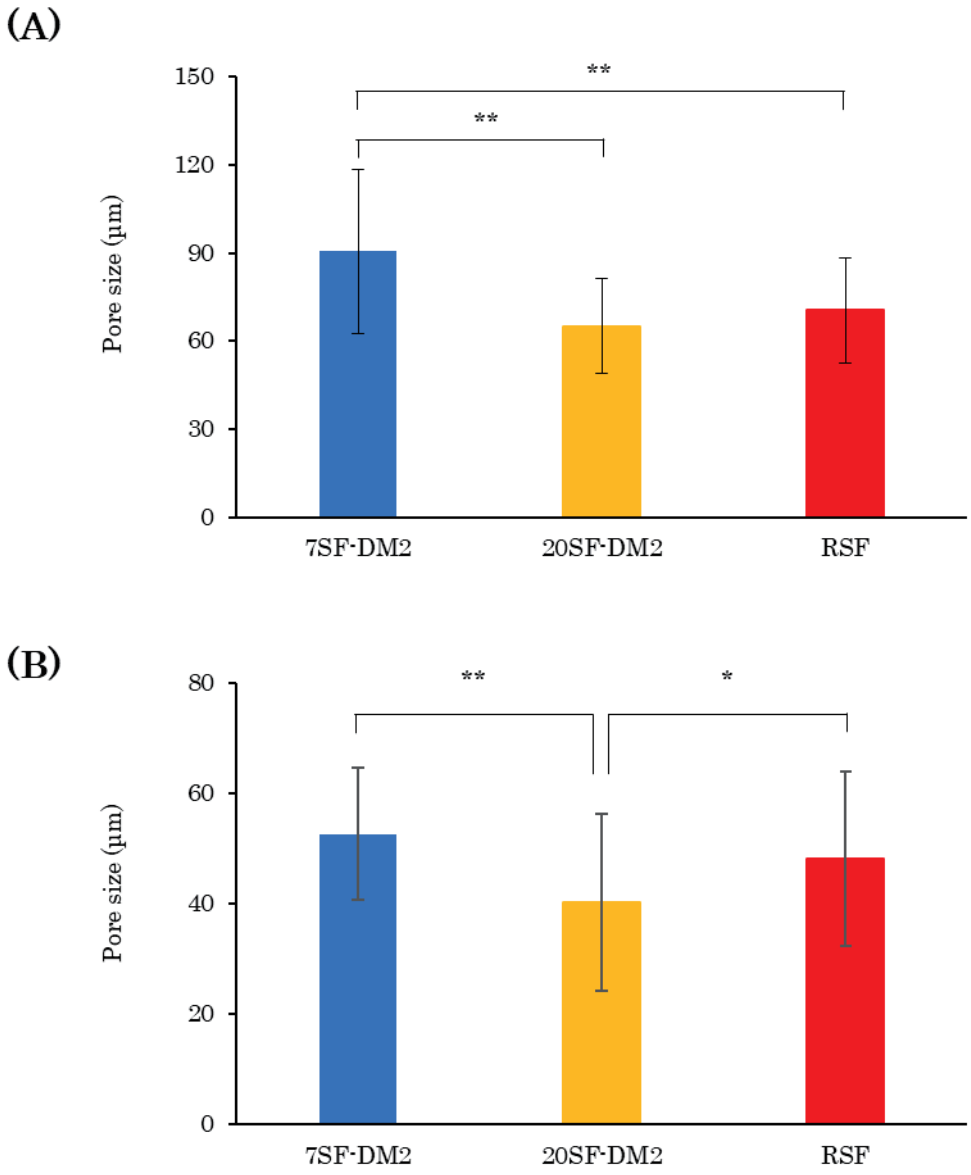

Figure 3-6. Pore sizes of sponges fabricated at (B) 2% (*w/v*) and (C) 4% (*w/v*) of SF aqueous solution. Pore size was measured using Image J from SEM images. Significance was inferred from results of *t*-test, shown as ** $p < 0.01$ and * $p < 0.05$ ($n = 50$).

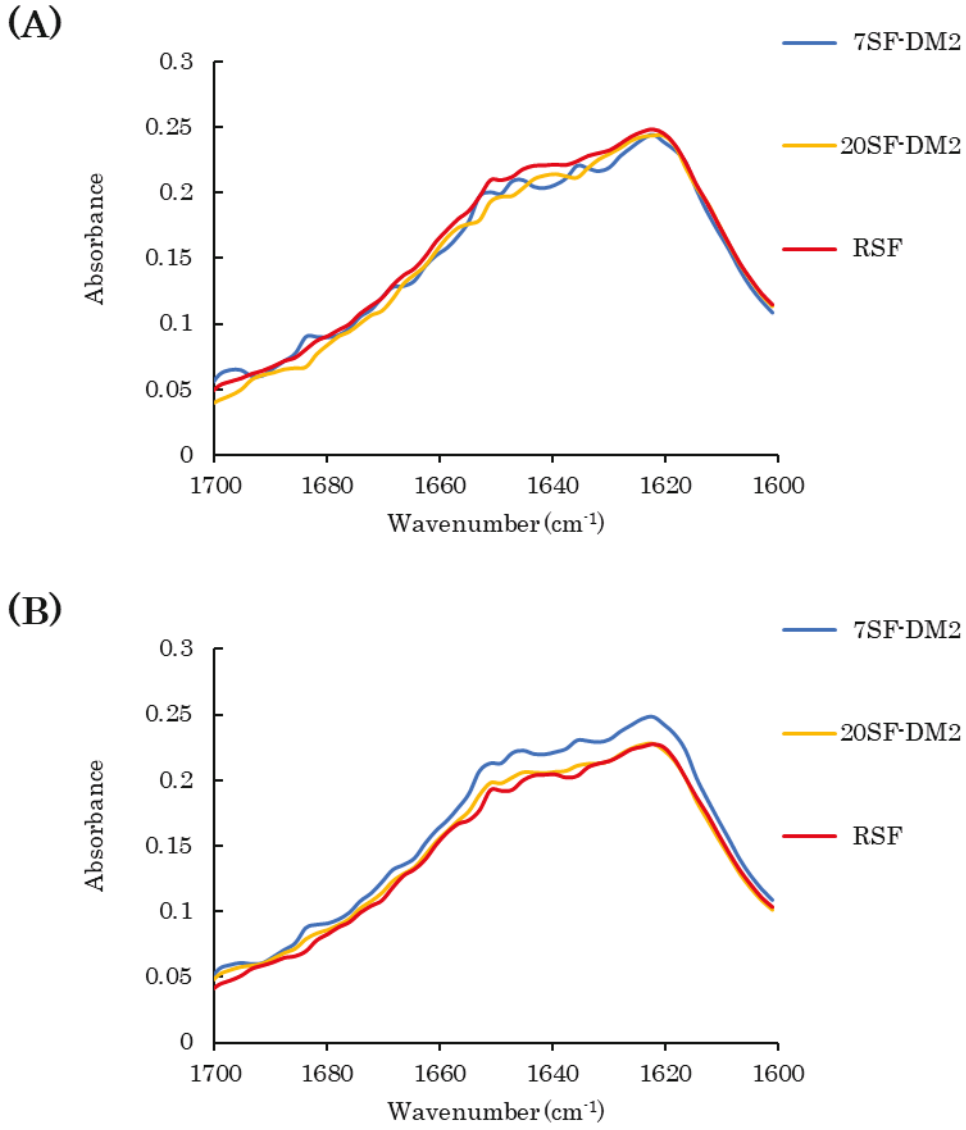

Figure 3-7. ATR-FTIR spectra at amide I region of sponges fabricated from (A) 2% (*w/v*) and (B) 4% (*w/v*) of 7SF-DM2, 20SF-DM2, and RSF solutions.

Table 3-1. Compressive moduli of sponges fabricated from (A) 2% (*w/v*) and (B) 4% (*w/v*) of fractionation 7SF-DM2, 20SF-DM2, and RSF solutions.

Sample	7SF-DM2, MPa	20SF-DM2, MPa	RSF, MPa
SF 2%	1.2 ± 0.09	1.1 ± 0.06	1.1 ± 0.1
SF 4%	1.3 ± 0.1	1.5 ± 0.05	1.2 ± 0.1

3.3. Conclusion

The fractionated SFs were available to fabricated to nanofiber nonwoven mats using electrospinning and to porous sponge structures using freeze–thaw method, similar to non-fractionated SFs. Although there was no influence of MW on the secondary structure and crystallinity of nanofibers and sponges, MW of SF affected the morphology and mechanical properties of the nanofibers and the sponges. The MW difference of SF within the range using fractionation of this study is not a crucially significant condition for fabrication of SF materials.

Chapter 4.

Gelation mechanism of silk fibroin aqueous solution

4.0. Introduction

Gelation mechanisms of regenerated silk fibroin (RSF) have been described in several reports. Ayub et al. reported the formation of ß-sheet structure through hydrogen bonding in RSF gel from an aqueous solution by adjusting the pH near the isoelectronic point of silk fibroin (SF) [119]. Kasoju et al. reported that gelation of an RSF aqueous solution using methanol (non-solvent) was induced by aggregation of RSF because of disturbances in the interactions between water and RSF through the exchange of methanol with water on RSF [71]. The gelation mechanism of accelerated gelation by ultrasonication was proposed as physical cross-links by the formation of initial interactions related to a ß-sheet triggered by sonication-induced change in hydrophobic hydration [27]. Matsumoto et.al. expressed the RSF gelation mechanism as three-stage model consisting of the following; 1. at fresh solution, a ß-sheet structure with negligible intermolecular bindings; 2. induction of gelation by weaker interactions such as hydrogen bonding; and 3. construction of a stable β-sheet structure irreversibly at the late stage of gelation [120]. Li et al. described the mechanism of gelation induced by soft freezing as self-assembly of RFS molecules because of decreased molecular mobility and increased concentration by dehydration [121]. These studies were undertaken to clarify the gelation mechanisms that when an RSF aqueous solution was given various stimuli, not investigate standing RSF aqueous solutions statically for storage. However, several phenomena related to changes of RSF molecules during storage have been reported. The presence of L-chains and the decrease of molecular weight (MW) of H-chains in RSF

aqueous solutions were influenced by storage time [122]. Cho et al. reported that RSF molecule decomposition occurred during storage and lower MW molecules accelerated RSF aggregation [123]. Zainuddin et al. used ^{1}H-NMR to analyze the changes of the secondary structures of RSF molecules to ß-strand during storage at 4 °C until gelation [124]. Nevertheless, no discussion of mechanism of gelation process during storage was found in these reports.

The objective of this study is to elucidate the gelation mechanisms of RSF aqueous solutions during storage without any stimuli. Firstly, the MW and MW distribution of SF molecules in RSF aqueous solution during storage was determined using GPC at various storage time. The hydrolyzed RSF aqueous solution was also used to elucidate the influence of MW on the gelation mechanism. The SF molecules particle size of RSF aqueous solution during storage was determined using dynamic light scattering (DLS), and viscosity of RSF aqueous solution was measured at various storage time to follow the estimation of forming particles. The changing secondary structures were evaluated by FTIR.

4.1. Materials and methods

4.1.1. Preparation of RSF aqueous solution

RSF aqueous solution was prepared from degummed silk thread thorough dissolution and dialysis process with the same method as section 2.1.1.. To prepare an RSF with lower molecules, the degummed silk fiber was hydrolyzed in 0.2 M $NaOH_{aq}$ at 60 °C for 1 hr. The hydrolyzed silk fiber was washed thoroughly with RO water and dried at 50 °C for at least 12 hr. As

described above, hydrolyzed RSF aqueous solution was prepared.

4.1.2. Storage and gelation

4% (*w/v*) RSF aqueous solution in a plastic tube was incubated at 4 °C and 60 °C until gelation, and 4% (*w/v*) hydrolyzed RSF aqueous solution was incubated at 60 °C. The sample names are designated as RSF4, RSF60 and RSF60-0.2, respectively.

In this study, the gelation time was defined as the time at which the RSF aqueous solution becomes white, turbid, and hold on its own when the container turn upside down [125].

4.1.3 Characterizations

4.1.3.1. Determination of MW

The MW of the RSF aqueous solution was determined for RSF4, RSF60 and RSF60-0.2 until gelation by GPC at predetermined days. The incubated RSF aqueous solutions were diluted to 0.1% (*w/v*) with an elution buffer. I assume that the effect of this elution buffer on MW determination was not important because MW was evaluated comparatively with the MW standard eluted by the same buffer. The measurement by GPC and the estimation of MW were performed under the conditions and methods as section 2.1.4..

4.1.3.2. RSF particle size distribution measurement

Particle size distribution measurement was performed by dynamic light scattering under the conditions as section 2.1.7. except the solution

concentration.

4.1.3.3. Viscosity measurements

The viscosity of sample aqueous solution was measured using oscillation type viscometer (VISCOMATE VM-10A series, SEKONIC CORPORATION, Tokyo, Japan). Samples were adjusted to concentration of 4% (*w/v*) and kept under r.t. before measurement. The measurement was repeated three times and the results were averaged.

4.1.3.4. Structure analysis

Sample aqueous solutions and gel were freeze-dried for measurement of the secondary structure of RSF4. The freeze-dried samples were analyzed using FTIR spectrometer under the conditions as section 2.1.10.. The FTIR spectra were measured, and the amide I (1600–1700 cm^{-1}) peaks of the FTIR spectra were decomposed and curve-fitted for analysis of the ß-sheet content with same method as section 2.1.10..

4.2. Results and Discussion

4.2.1. Gelation of RSF aqueous solution during storage

The gelation time of RSF aqueous solution during storage at 4 °C was shown in Figure 4-1. From my experiments, the gelation time was observed to be varied from 36 to 172 days. The change of the gelation time might derive from subtle differences in the preparation condition of the RSF aqueous solution such as dissolution [126] and dialysis processes [127]. To clarify the

gelation mechanism according to storage time, the percentage of gelation time (%GT) was defined to analyze the properties of the RSF aqueous solution during storage until gelation. After completion of measurements until gelation, the days of measurements were calculated to %GT using gelation day. For example, 10%GT means 10 days of storage time when gelation occurred at 100 days after starting storage. Hereinafter, %GT is used as the storage time.

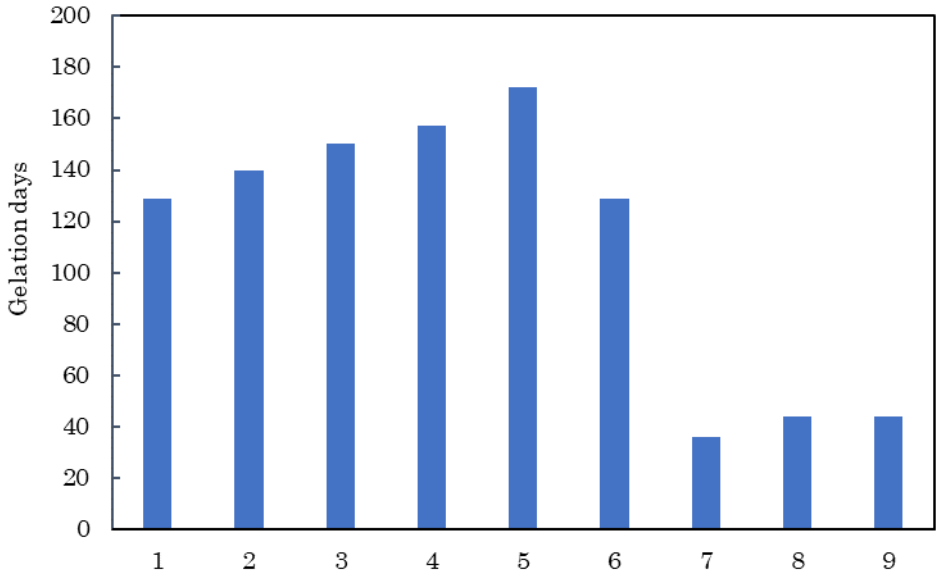

Figure 4-1. Gelation times of RSF aqueous solutions at 4 °C (RSF4) for the respective experiments (repeated nine times).

4.2.2. Molecular size change of RSF during storage

After performing GPC measurements of the RSF aqueous solutions after various storage times at 4 °C, the elution profiles were summarized in Figure 4-2. Two peaks appeared in each GPC profile of RSF aqueous solution at various storage time. The peaks at around 6.5 min retention time present

the accumulated molecules with higher MW than the exclusion limit of the GPC column. The molecular size decrease according to storage time was observed. The cleavage of molecules in the RSF aqueous solution during storage at 4 °C was reported by Salvador et al. [122]. Changes of M_p (MW at elution peak estimated from standard), M_w (weight-averaged molecular weight calculated with the elution profile), M_n (number-averaged molecular weight calculated with the elution profile), and PDI (polymer dispersion index, M_w/M_n) according to the storage time were shown in Figure 4-3. The value of M_w at the initial storage time was estimated at around 130 kDa and it was lower than 350 kDa of the theoretical H-chain M_w in silk glands [86,87]. That finding can be explained by the cleavage of molecules during degumming [88] and dissolution processes [91]. Actually, M_p and M_n decreased gradually until 50 to 70%GT and then decreased rapidly near gelation. However, M_w increased slightly according to storage time until 50 %GT, and then it decreased rapidly similarly to M_p and M_n. The decrease of M_p and M_n during storage is explainable by the cleavage of molecules. The M_w increase until 50%GT might be observed by the molecular association. Since M_w is more sensitive to molecules with higher molecular size than M_n is [100], the apparent larger molecules by the molecular association will more strongly influence M_w, although M_p and M_n decreased. As the result of the molecular size changes, PDI increased according to storage. This result indicates that cleavage of molecules and decreased molecular size are important factors affecting the gelation of RSF aqueous solution during storage at 4 °C.

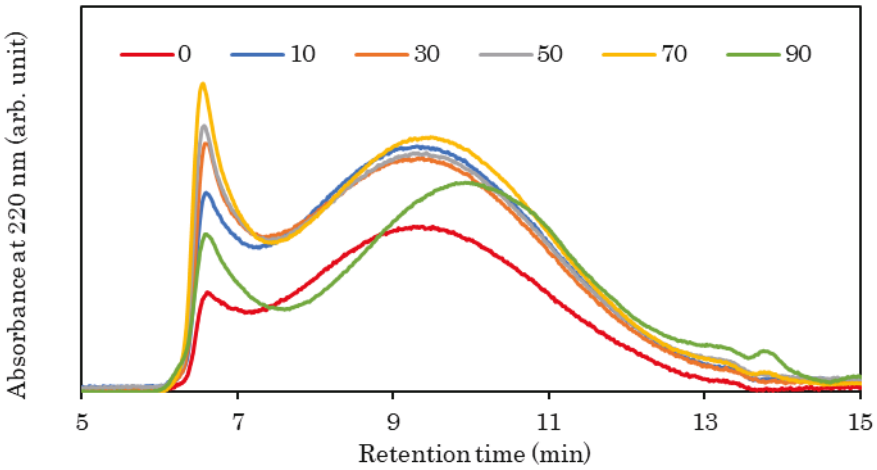

Figure 4-2. GPC elution profiles of RSF aqueous solution stored at 4 °C (RSF4). GPC was measured in RSF aqueous solutions at 0, 10, 30, 50, 70 and 90%GT (percentage of gelation time).

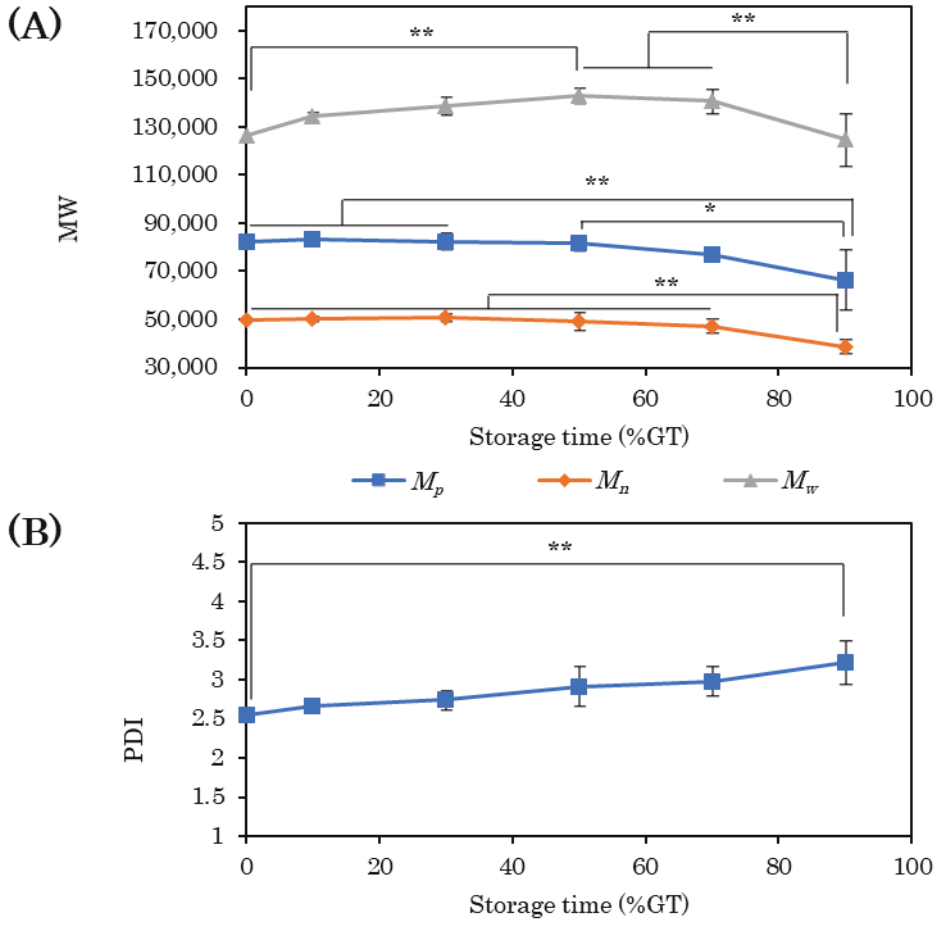

Figure 4-3. Difference of (A): Molecular weight at peak time (M_p), Number average molecular weight (M_n), and Weight average molecular weight (M_w) and (B): Polymer dispersion index (PDI) against storage time at 4 °C. (*: $p<0.05$, **: $p<0.01$, by Tukey-Kramer test, $n=4$).

4.2.3. Influence of storage temperature on gelation

RSF aqueous solutions were incubated at 60 °C to elucidate the effects of storage temperature on the gelation process. Gelation was observed after 12 days of incubation and the time of gelation was constant among the four times experiments. The storage temperature strongly influenced on the gelation behavior; higher temperature accelerated the gelation process as previous report [68]. Figure 4-4 (A) shows elution profiles of RSF aqueous solutions at different storage times under incubation at 60 °C. The elution curves were more clearly shifted to low molecular size according to storage time than in the profiles of storage at 4 °C shown in Figure 4-2. Figure 4-5 presented the changes of M_p, M_w, M_n, and PDI of RSF incubated at 60 °C against storage time. Compared with RSF stored at 4 °C, M_p, M_w, and M_n decreased greatly according to storage time. Increasing M_w by storage for RSF incubated at 60 °C was not observed. These differences between storage at 4 °C and 60 °C are expected to derive from both the rate of hydrolysis and the molecular motility of RSF. Higher temperatures can accelerate the hydrolysis of protein molecules, resulting in proceeding the cleavage of molecules and decreasing the molecular size. Consequently, M_p and M_n decreased more greatly by storage at 60 °C than 4 °C. It will become more difficult to associate molecules at 60 °C than at 4 °C, because molecules in aqueous solution can move more actively at 60 °C than at 4 °C. Therefore, M_w of RSF incubated at 60 °C decreased because of inhibition of molecular association to form large size molecules. PDI increased according to storage time similarly to results obtained at 4 °C. These results suggest that the smaller molecular size is a

crucially important factor in understanding the mechanism of gelation by storage of RSF aqueous solution.

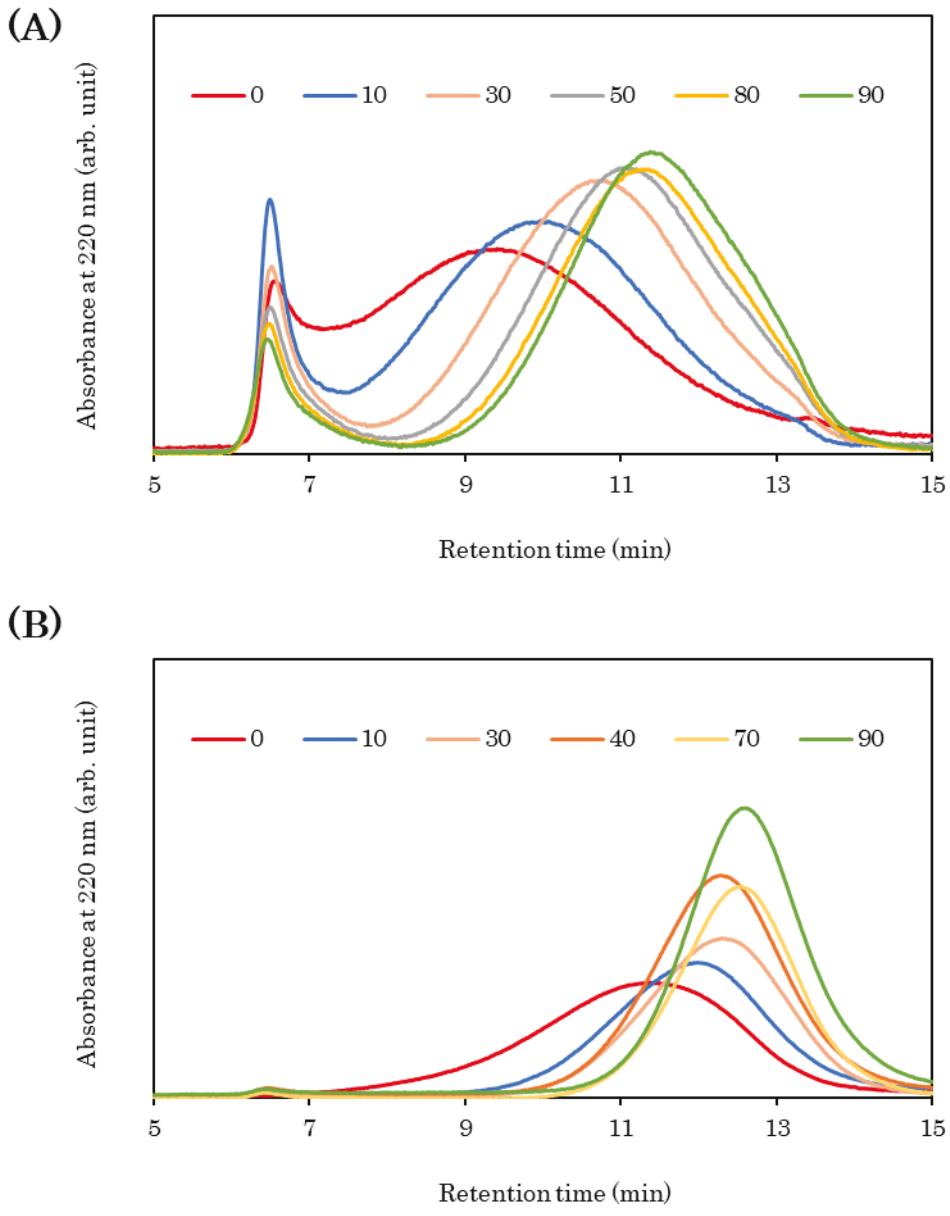

Figure 4-4. (A): GPC elution profiles of RSF60 aqueous solution at various storage time. (B): GPC elution profiles of RSF60-0.2 aqueous solution at various storage time.

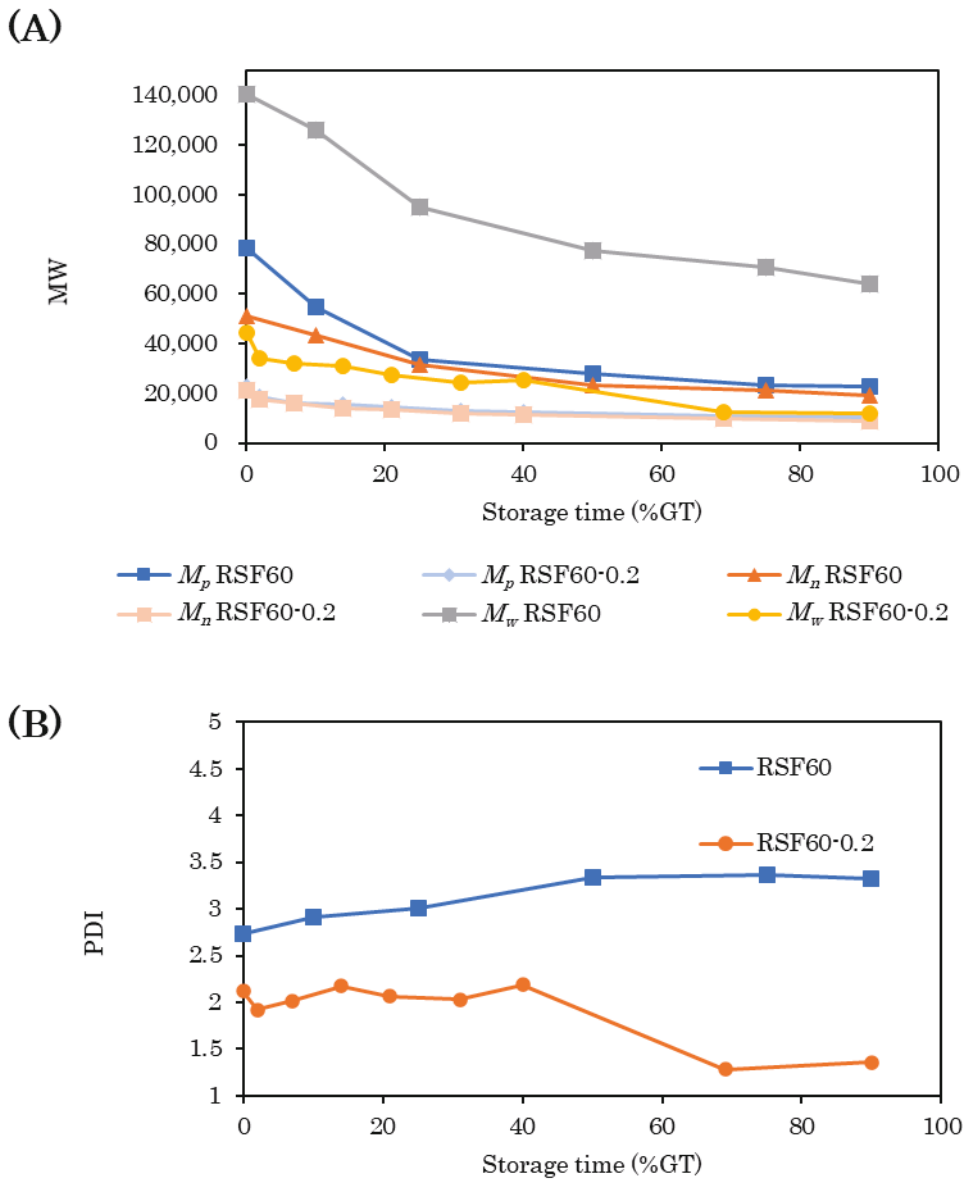

Figure 4-5. (A): Change of molecular weight at peak time (M_p), number average molecular weight (M_n) and weight average molecular weight (M_w) of RSF60 and RSF60-0.2 according to storage time. (B): Change of PDI of RSF60 and RSF60-0.2 according to storage time.

4.2.4. Gelation of hydrolyzed RSF

To confirm the dependence of molecular size decrease on gelation of the RSF aqueous solution, hydrolyzed RSF was used as the starting solution for elucidating the mechanism of gelation during storage. Although the non-hydrolyzed RSF aqueous solution was gelled for 12 days at 60 °C, no gelation was observed until 45 ± 2 days of incubation at 60 °C. However, the hydrolyzed RSF aqueous solution became white turbid and strongly aggregated as impossible to measurements, and these days were determined as %GT for RSF 60-0.2. The changes of M_p, M_w, M_n, and PDI with incubation time (%GT, in this case 100 %GT means 12 days) at 60 °C, which were calculated using the elution profiles shown in Figure 4-4 (B), are presented in with the results of non-hydrolyzed RSF (Figure 4-5).The molecular size of the hydrolyzed RSF decreased according to the incubation time, similarly to the results obtained for the non-hydrolyzed RSF, but the estimated MW of the hydrolyzed RSF was much different from that of the non-hydrolyzed RSF, not only at initial incubation, but also at near gelation. The MW (M_p, M_n, and M_w) of the hydrolyzed RSF at the initial gelation time was similar to, or at least not higher than that of the non-hydrolyzed RSF at near gelation. Further in contradiction to the result for PDI of non-hydrolyzed RSF, decrease of PDI along with incubation time was observed. This finding indicates that the molecular size dispersion narrowed during incubation in the case of the hydrolyzed RSF. Consideration of these results together suggest that the coexistence of both large and small size molecules in the solution is required for the gelation during storage.

4.2.5. Formation particles during storage

Figure 4-6 shows the results of the particle size distribution existing in an RSF aqueous solution during incubation at 60 °C measured by DLS. No clear peak of particle size was observed in the RSF aqueous solution before incubation (Figure 4-6 (A)), but particles appeared during incubation and the particle size was estimated around 100 to 400 nm as shown in Figure 4-6 (D), E and F. In hydrolyzed RSF aqueous solution also, particles were formed by incubation. The particle size was determined around 100 to 400 nm as shown in Figure 4-7 (E) and (F). Cho et al. reported that particles were formed in the aqueous solution by decreased the molecular size under the different dissolution conditions, and the particle size was estimated at 100 to 300 nm [123]. The similar results were confirmed in my study, and particles will be formed by small molecules appearing during storage. Smaller molecular size RSF in hydrolyzed RSF aqueous solution could form particles at the beginning as shown in Figure 4-7 (A) and during storage, similarly with non-hydrolyzed RSF. However, no gelation in the hydrolyzed RSF aqueous solution was observed. This result indicates that the gelation of the RSF aqueous solution during storage requires construction of a network by larger molecules with particles formed by small molecules. Cho et al. reported that the necessity of large size molecules to build a network with neighboring molecules [126]. The viscosity change of RSF aqueous solution during storage was shown in Figure 4-8. The viscosity decreased along with storage time until gelation. The decrease of the solution viscosity during storage is explained by the cleavage of molecules and the formation of particles. Figure

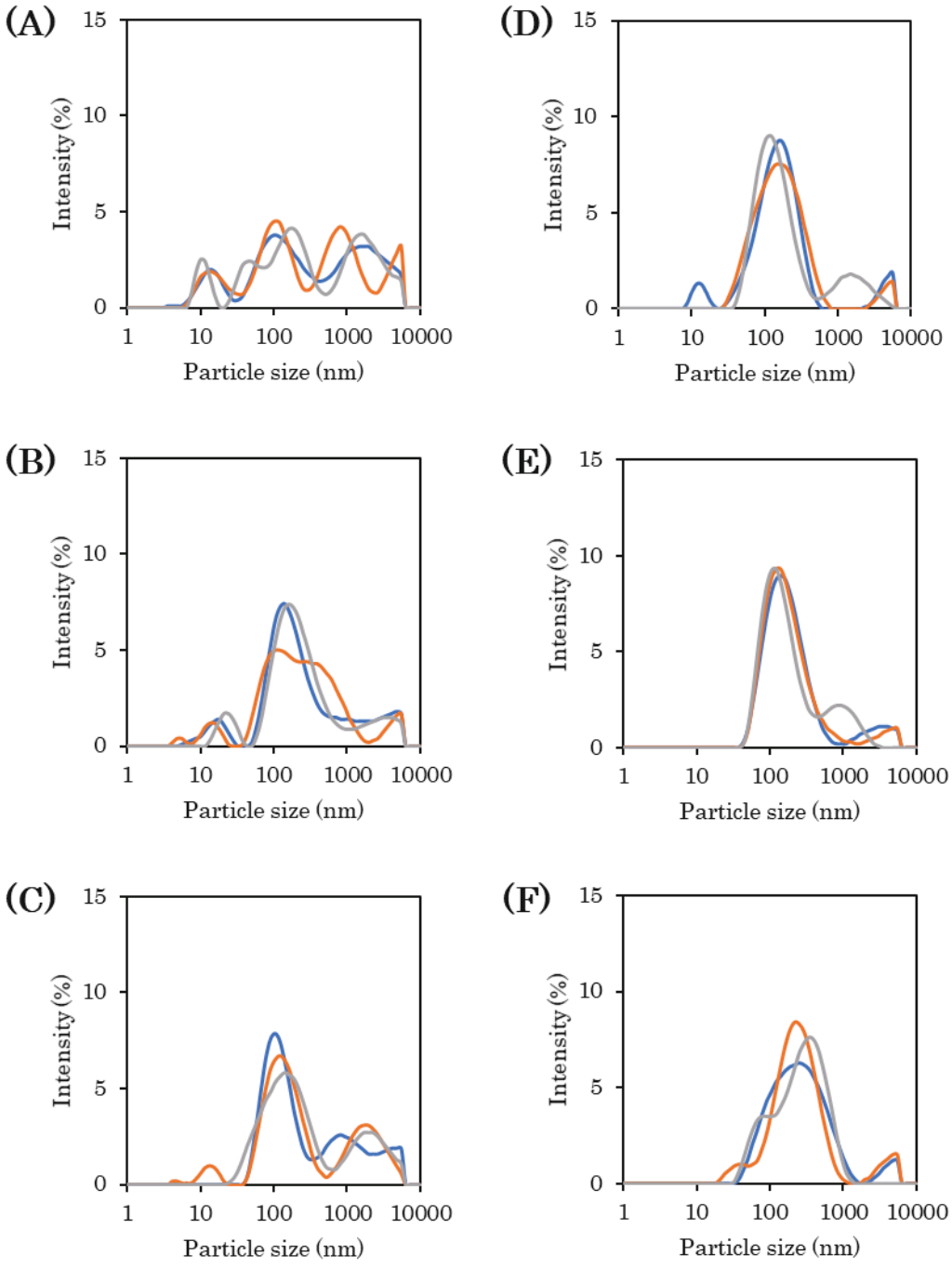

Figure 4-6. Particle size distributions in RSF60 aqueous solutions during storage. Measurements were taken three times for each sample: (A) at 0%GT, (B) at 10%GT, (C) at 30%GT, (D) at 60%GT, (E) at 80%GT, and (F) at 90%GT.

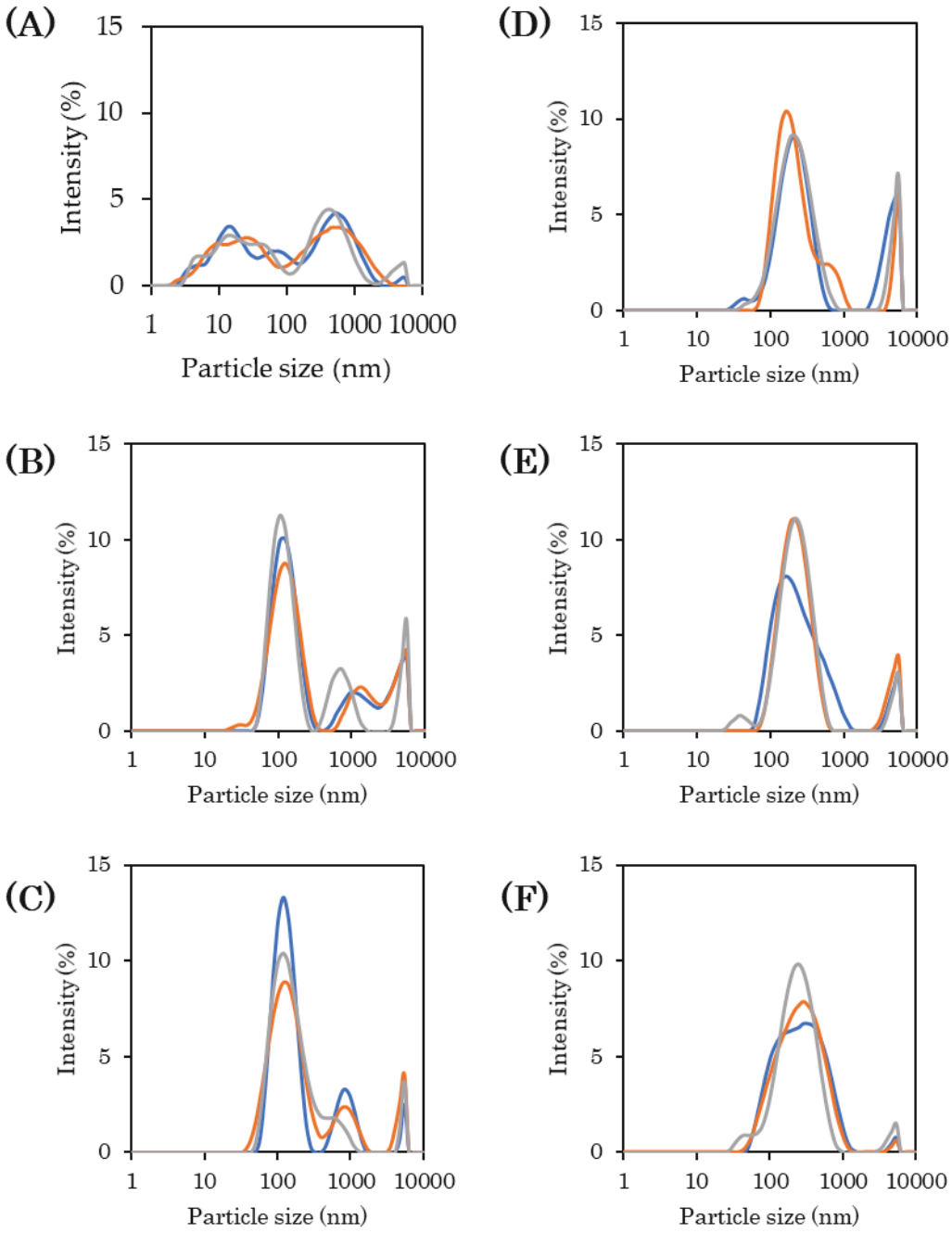

Figure 4-7. Particle size distributions in RSF60-0.2 aqueous solutions during storage. Measurements were taken three times for each sample: (A) at 0%GT, (B) at 20%GT, (C) at 30%GT, (D) at 40%GT, (E) at 60%GT, and (F) at 90%GT.

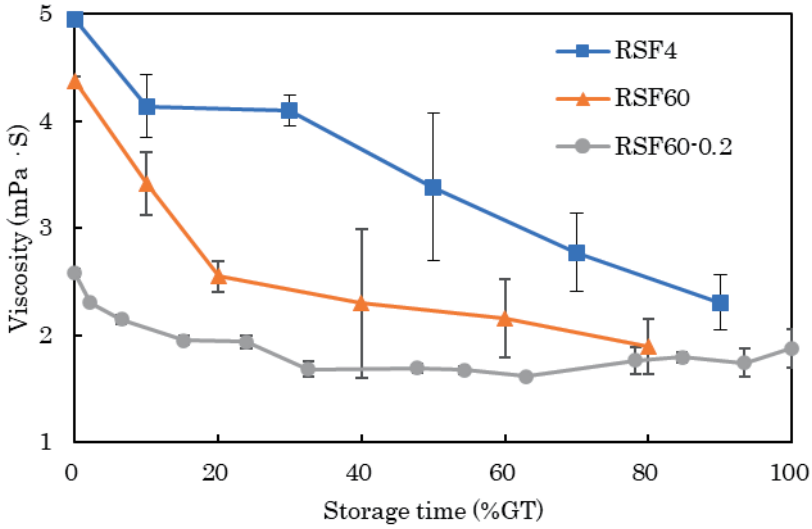

Figure 4-8. Effects of storage time on viscosities of RSF4, RSF60, and RSF60-0.2 aqueous solutions.

4-9 (A) shows the ß-sheet structure ratio and (B) shows random and α-helix structure respectively of freeze-dried RSF from the aqueous solution stored at 4 °C at various storage time estimated by ATR-FTIR spectrum (Figure 4-10). Ratio of ß-sheet structure increased gradually by storage until near the point of gelation. Then the gel after gelation contained a high ratio ß-sheet structure as earlier reports [120,122,124]. The ratio of random and α-helix structure was decreased with increasing the ratio of β-sheet structure during storage time. These results indicate that the molecular assembly and appearance of particles were induced by formation of the ß-sheet structure, which is the secondary structure consisting of crystal parts of silk, from the random and a-helix structure.

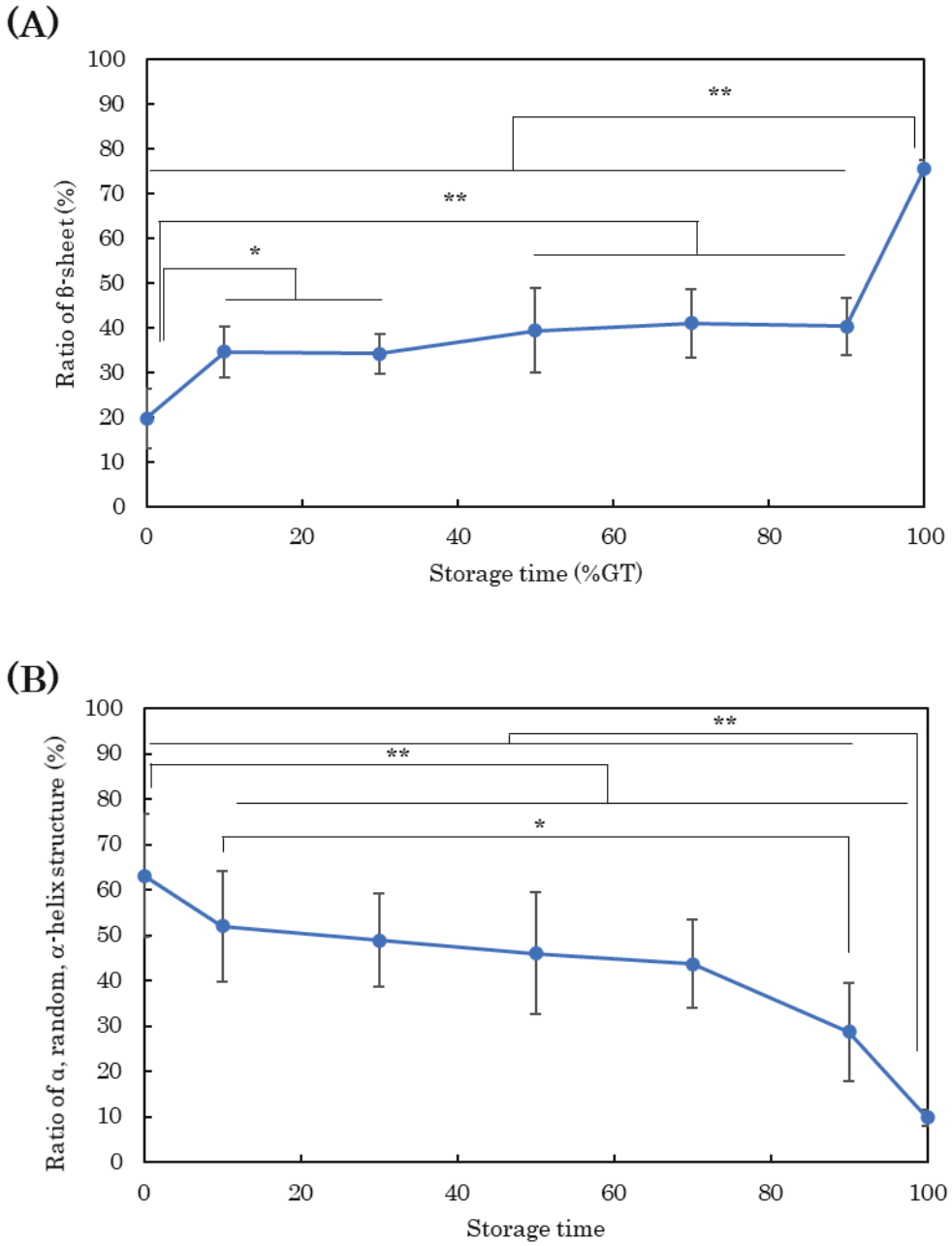

Figure 4-9. Effects of storage time on (A) ß-sheet structure ratio and (B) random and a-helix structure, of freeze-dried RSF from aqueous solutions at various storage times, ß-sheet ratio and random and a-helix ratio were calculated from amide I peak in the ATR-FTIR spectrum (*$p < 0.05$, **$p < 0.01$, n=5 by Tukey-Kramer test).

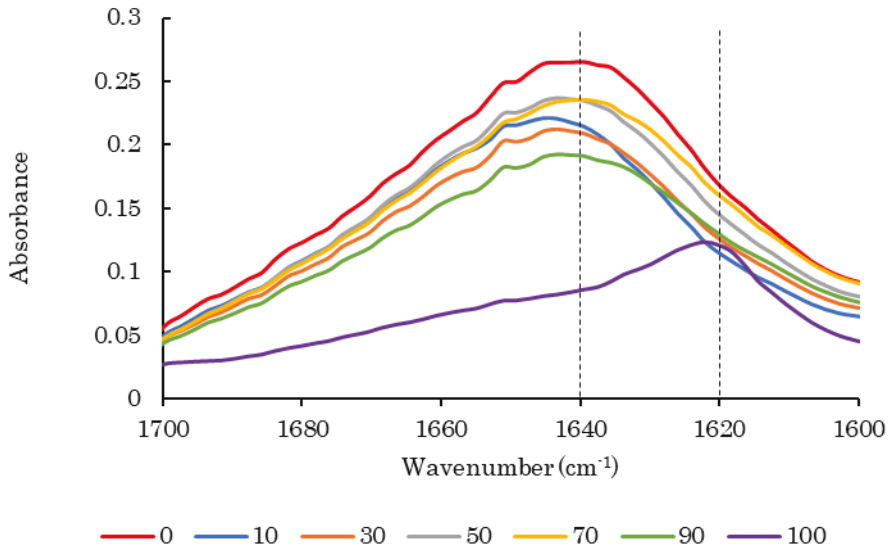

Figure 4-10. ATR-FTIR spectrum of freeze-dried RSF from the aqueous solution with various storage time.

4.2.6. Mechanism of gelation during storage

Figure 4-11 shows a schematic drawing showing the gelation mechanism of an RSF aqueous solution during storage inferred from results of this study. RSF molecules are cleaved by hydrolysis in the aqueous solution at the initial stage of storage. Small molecules appear and increase in the aqueous solution according to the storage time. The small molecules become associated with other molecules through interaction by β-sheet structure. The assembled molecules form particles with size of 100–400 nm. Then, the particle number increases concomitantly with the increase of small molecules according to storage time. Finally, at approximately the gelation time, larger molecules remaining in the solution will construct a network with the particles and the gelation will be completed. Therefore, the gelation time of the RSF aqueous solution will be mainly depended on the cleavage rate of

RSF molecules during storage.

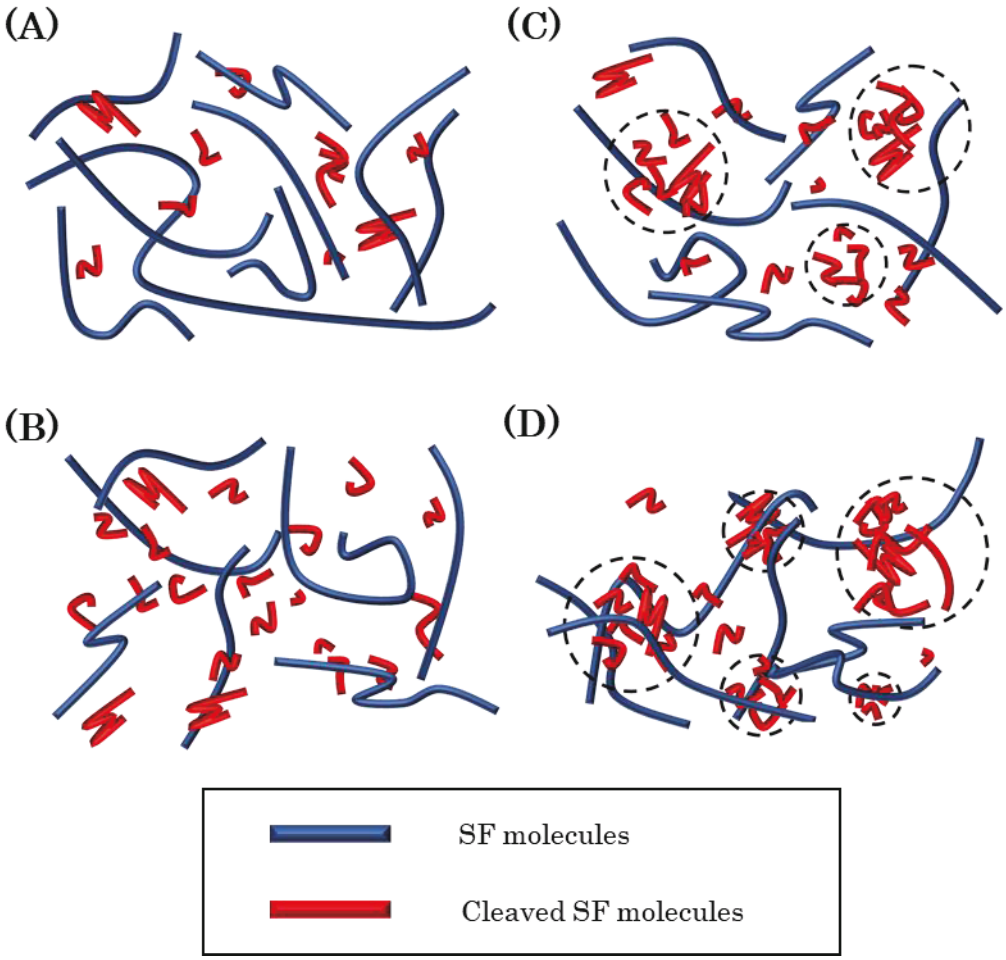

Figure 4-11. Schematic drawing of the gelation mechanism of RSF aqueous solution during storage. (A) Fresh RSF aqueous solution. (B) Increase smaller size SF molecules created by cleavage. (C) Smaller SF molecules form particles by ß-sheet structure formation. (D) Particles interact with larger RSF molecules; a molecular network is constructed to make gel.

4.3. Conclusion

The mechanism of gelation of RSF aqueous solution was investigated when it was stored without any stimulation. The decrease in the molecular size of RSF and the formation of particles in the aqueous solution during

storage were observed by GPC and DLS measurements, respectively. No gelation was observed in the hydrolyzed RSF aqueous solution, which is mainly composed of RSF with small molecular size. Further viscosity of the RSF aqueous solution decreased according to storage time. The increasing ratio of ß-sheet structure of the freeze-dried RSF aqueous solution during storage was found by FTIR measurement. From these results, it is indicated that the SF molecular size should be considered for the gelation mechanism of RSF aqueous solution during storage.

Chapter 5.

Conclusion

In this study, fractionation of regenerated silk fibroin (RSF) was successfully achieved by use of ammonium sulfate (AS) precipitation method and it was revealed that the appropriate process of AS precipitation was to use a dialysis membrane at 4 °C. No clear differences of the processability from the fractionated RSF solution to film, sponge, and nanofiber were presented on the MW changes, while the morphology and mechanical properties were influenced by the MW of the fractionated RSF. These results will be important information to fabricate RSF materials. But, since it was difficult to control the MW distributions of each fractionated RSF by AS precipitation method even with the improved process, clear separation of each fraction was impossible to get the narrow MW distribution RSF which are minimized the MW overlapping among each fraction. In order to reveal the effects of the MW on the various properties of RSF materials more precisely, the MW fractions of RSF with narrower MW distribution will be required.

Gelation of RSF aqueous solution during storage is crucial problem to commercialize RSF productions fabricated industrially from RSF aqueous solution. In this study, the gelation mechanism focused on the MW changes of RSF in the aqueous solution during storage was proposed. The cleavage of RSF molecules in the aqueous solution occurred by hydrolysis during storage even at 4 °C and lower molecular size RSF molecules increased in the solution according to the storage time. The increased small molecules form the molecular aggregations spontaneously through β-sheet structure formation, and then a molecular network among the remained larger size molecules with the aggregation particles as the crosslinking points is formed and the RSF

aqueous solution turn to the gel consequently. There are three key reactions in order to prevent gelation of the RSF aqueous solution during storage, which are 1) inhibition of molecular cleavage, 2) prevention of aggregation among the small molecules, and 3) interference of the molecular network formation. Among them the inhibition of molecular cleavage will be effective for preventing the gelation and it may be a possible method for storage that the RSF aqueous solution is stored at lower temperature without freezing as possible to minimize the hydrolysis of RSF molecules. But further study is required for determining an industrial appropriate way for storage of RSF aqueous solution.

Acknowledgements

I express my sincere gratitude to Prof. Yasushi Tamada (Division of Applied Biology, Faculty of Textile Science and Technology, Shinshu University) for his enthusiastic guidance and support as my supervisor in this research.

I appreciate Ass. prof. Mitsumasa Osada (Division of Chemistry and Materials) for helping amino acid analysis.

I'm grateful to Prof. Makoto Shimosaka (Division of Applied Biology), Ass. prof. Tomoko Hashimoto (Division of Applied Biology), Prof. Yasuo Gotoh (Division of Chemistry and Materials), Dr. Hidetoshi Teramoto (National Agriculture and Food Research Organization (NARO)), and Prof. Thomas Rosenau (University of Natural Resources and Life Sciences Vienna (BOKU)) for reviewing of this dissertation.

B.Sc. Yu Masuda and B.Sc. Kota Ishikawa contributed to the methodology and the investigation in chapter 2, respectively, and I gratefully acknowledge the work of past and present members of Tamada laboratory.

This research was supported by Grant-in-Aid for the Shinshu University Advanced Leading Graduate Program by the Ministry of Education, Culture, Sports, Science and Technology (MEXT), Japan. This work was funded by Shinshu University and JSPS KAKENHI grant number JP19H04466.

Last but certainly not least, I would like to thank my family for their continuous support and encouragement throughout my long years of university life.

References

1. Altman, G.H.; Diaz, F.; Jakuba, C.; Calabro, T.; Horan, R.L.; Chen, J.; Lu, H.; Richmond, J.; Kaplan, D.L. Silk-Based Biomaterials. *Biomaterials*, *24*, 401–416, 2003.

2. Porter, D.; Vollrath, F. Silk as a Biomimetic Ideal for Structural Polymers. *Adv Mater*, *21*, 487–492, 2009.

3. Kaplan, D.; Adams, W.; Farmer, B.; Viney, C. Silk: Biology, Structure, Properties, and Genetics. Silk Polymers, *ACS Symposium Series*, 544, 2-16, 1993.

4. Kaplan, D.L.; Fossey, S.; Viney, C.; Muller, W. Self-Organization (Assembly) in Biosynthesis of Silk Fibers - A Hierarchical Problem. *Mrs Online Proc Libr, 255*, 19–29, 1991.

5. Rozet, S.; Tamada, Y. An Improved Process for Stably Preparing of Antheraea Pernyi Fibroin Aqueous Solution. *J Silk Sci Technology Jpn*, *27*, 23–31, 2019.

6. Sponner, A.; Vater, W.; Monajembashi, S.; Unger, E.; Grosse, F.; Weisshart, K. Composition and Hierarchical Organisation of a Spider Silk. *Plos One*, 2(10), e998, 2007.

7. Kameda, T.; Kojima, K.; Miyazawa, M.; Fujiwara, S. Film Formation and Structural Characterization of Silk of the Hornet Vespa Simillima Xanthoptera Cameron. *Zeitschrift Für Naturforschung C*, *60*, 906–914, 2005.

8. Yoshioka, T.; Tsubota, T.; Tashiro, K.; Jouraku, A.; Kameda, T. A Study of the Extraordinarily Strong and Tough Silk Produced by Bagworms. *Nat Commun.*, *10*, 1469, 2019.

9. Zhao, H.-P.; Feng, X.-Q.; Shi, H.-J. Variability in Mechanical Properties of Bombyx Mori Silk. *Mater Sci Eng C*, *27*, 675–683, 2007.

10. Tamada, Y. Utilization of Silk as Biomaterials. *Nippon Gomu Kyokaishi*, *87*, 428–433, 2014.

11. Putthanarat, S.; Eby, R.K.; Naik, R.R.; Juhl, S.B.; Walker, M.A.; Peterman, E.; Ristich, S.; Magoshi, J.; Tanaka, T.; Stone, M.O.; Farmer, B.L.; Brewer, C.; Ott, D. Nonlinear Optical Transmission of Silk/Green Fluorescent Protein (GFP) Films. *Polymer*, *45*, 8451–8457, 2004.

12. Li, J.; Ye, L.; Che, J.; Song, J.; You, Z.; Yun, K.; Wang, S.; Zhong, B. Comparative Proteomic Analysis of the Silkworm Middle Silk Gland Reveals the Importance of Ribosome Biogenesis in Silk Protein Production. *J Proteomics*, *126*, 109–120, 2015.

13. Zhang, Y.-Q. Applications of Natural Silk Protein Sericin in Biomaterials. *Biotechnol Adv*, *20*, 91–100, 2002.

14. Kunz, R.I.; Brancalhão, R.M.C.; Ribeiro, L. de F.C.; Natali, M.R.M. Silkworm Sericin: Properties and Biomedical Applications. *Biomed Res Int*, *2016*, 8175701, 2016.

15. Asakura, T.; Sugino, R.; Okumura, T.; Nakazawa, Y. The Role of Irregular Unit, GAAS, on the Secondary Structure of Bombyx Mori Silk Fibroin Studied with 13C CP/MAS NMR and Wide - angle X - ray Scattering. *Protein Sci*, *11*, 1873–1877, 2002.

16. Ha, S.-W.; Gracz, H.S.; Tonelli, A.E.; Hudson, S.M. Structural Study of Irregular Amino Acid Sequences in the Heavy Chain of Bombyx m Ori Silk Fibroin. *Biomacromolecules*, *6*, 2563–2569, 2005.

17. Hakimi, O.; Knight, D.P.; Vollrath, F.; Vadgama, P. Spider and Mulberry Silkworm Silks as Compatible Biomaterials. *Compos Part B Eng*, *38*, 324–337, 2007

18. Mori, H.; Tsukada, M. New Silk Protein: Modification of Silk Protein by Gene Engineering for Production of Biomaterials. *Rev Mol Biotechnology*, *74*, 95–103, 2000.

19. Horan, R.L.; Antle, K.; Collette, A.L.; Wang, Y.; Huang, J.; Moreau, J.E.; Volloch, V.; Kaplan, D.L.; Altman, G.H. In Vitro Degradation of Silk Fibroin. *Biomaterials*, *26*, 3385–3393, 2005.

20. Meinel, L.; Hofmann, S.; Karageorgiou, V.; Kirker-Head, C.; McCool, J.; Gronowicz, G.; Zichner, L.; Langer, R.; Vunjak-Novakovic, G.; Kaplan, D.L. The Inflammatory Responses to Silk Films in Vitro and in Vivo. *Biomaterials*, *26*, 147–155, 2005.

21. Thurber, A.E.; Omenetto, F.G.; Kaplan, D.L. In Vivo Bioresponses to Silk Proteins. *Biomaterials*, *71*, 145–157,2015.

22. Tamada, Y. メディカルマテリアルとしてのシルク. *SANSHI-KONCHU BIOTEC,* 86(1), 3-11, 2017.

23. Kunz, R.I.; Brancalhão, R.M.C.; Ribeiro, L. de F.C.; Natali, M.R.M. Silkworm Sericin: Properties and Biomedical Applications. *Biomed Res Int*, *2016*, 8175701, 2016.

24. Lamboni, L.; Gauthier, M.; Yang, G.; Wang, Q. Silk Sericin: A Versatile Material for Tissue Engineering and Drug Delivery. *Biotechnol Adv*, *33*, 1855–1867, 2015.

25. Fine, N.A.; Lehfeldt, M.; Gross, J.E.; Downey, S.; Kind, G.M.; Duda, G.; Kulber, D.; Horan, R.; Ippolito, J.; Jewell, M. SERI Surgical Scaffold, Prospective Clinical Trial of a Silk-Derived Biological Scaffold in Two-Stage Breast Reconstruction. *Plast Reconstr Surg*, *135*, 339–351, 2015.

26. Karageorgiou, V.; Meinel, L.; Hofmann, S.; Malhotra, A.; Volloch, V.; Kaplan, D. Bone Morphogenetic Protein ‐ 2 Decorated Silk Fibroin Films Induce Osteogenic Differentiation of Human Bone Marrow Stromal Cells. *J Biomed Mater Res A*, *71A*, 528–537, 2004.

27. Wang, X.; Kluge, J.A.; Leisk, G.G.; Kaplan, D.L. Sonication-Induced Gelation of Silk Fibroin for Cell Encapsulation. *Biomaterials*, *29*, 1054–1064, 2008.

28. Kambe, Y.; Kojima, K.; Tamada, Y.; Tomita, N.; Kameda, T. Silk Fibroin Sponges with Cell Growth ‐ promoting Activity Induced by Genetically Fused Basic Fibroblast Growth Factor. *J Biomed Mater Res A*, *104*, 82–93, 2016.

29. Min, B.-M.; Lee, G.; Kim, S.H.; Nam, Y.S.; Lee, T.S.; Park, W.H. Electrospinning of Silk Fibroin Nanofibers and Its Effect on the Adhesion and Spreading of Normal Human Keratinocytes and Fibroblasts in Vitro. *Biomaterials*, *25*, 1289–1297, 2004.

30. Magoshi, J. 絹フィブロインの転移機構. Kobunshi Ronbunshu, *31*, 765–770, 1974.

31. Konishi, T.; Kim, D.K.; Itoh, T. Structure of the Drawn and Annealed Silk Fibroin Films. *Sen'i Gakkaishi*, *53*, 365–372, 1997.

32. Tamada, Y.; Ikada, Y. Cell Attachment to Various Polymer Surfaces. In *Polymers in Medicine II*; Chiellini, E., Giusti, P., Migliaresi, C., Nicolais, L., Eds.; Springer: Boston, MA, USA, *34*, 101–115, 1986.

33. Tamada, Y.; Ikada, Y. Fibroblast Growth on Polymer Surfaces and Biosynthesis of Collagen. *J Biomed Mater Res*, *28*, 783–789, 1994.

34. Liu, T.; Miao, J.; Sheng, W.; Xie, Y.; Huang, Q.; Shan, Y.; Yang, J. Cytocompatibility of Regenerated Silk Fibroin Film: A Medical Biomaterial Applicable to Wound Healing. *J Zhejiang Univ Sci B*, *11*, 10–16, 2010.

35. Langer, R.; Vacanti, J.P. Tissue Engineering. *Science*, *260*, 920–926, 1993.

36. Nishida, T.; Yasumoto, K.; Otori, T.: Desaki, J. The Network Structure of Corneol Fibroblasts in the Rot as Revealed by Scanning Electron microscopy. *Investig. Ophthalmol. Vis. Sci.*, 29, 1887–1890, 1988.

37. Kim, H.J.; Kim, U.-J.; Vunjak-Novakovic, G.; Min, B.-H.; Kaplan, D.L. Influence of Macroporous Protein Scaffolds on Bone Tissue Engineering from Bone Marrow Stem Cells. *Biomaterials*, *26*, 4442–4452, 2005.

38. Meinel, L.; Karageorgiou, V.; Hofmann, S.; Fajardo, R.; Snyder, B.; Li, C.; Zichner, L.; Langer, R.; Vunjak - Novakovic, G.; Kaplan, D.L. Engineering Bone - like Tissue in Vitro Using Human Bone Marrow Stem Cells and Silk Scaffolds. *J Biomed Mater Res A*, *71A*, 25–34, 2004.

39. Meinel, L.; Hofmann, S.; Karageorgiou, V.; Zichner, L.; Langer, R.; Kaplan, D.; Vunjak - Novakovic, G. Engineering Cartilage - like Tissue Using Human Mesenchymal Stem Cells and Silk Protein Scaffolds. *Biotechnol Bioeng*, *88*, 379–391, 2004.

40. Morita, Y.; Tomita, N.; Aoki, H.; Sonobe, M.; Wakitani, S.; Tamada, Y.; Suguro, T.; Ikeuchi, K. Frictional Properties of Regenerated Cartilage in Vitro. *J Biomech*, *39*, 103–109, 2006.

41. Kambe, Y.; Yamamoto, K.; Kojima, K.; Tamada, Y.; Tomita, N. Effects of RGDS Sequence Genetically Interfused in the Silk Fibroin Light Chain Protein on Chondrocyte Adhesion and Cartilage Synthesis. *Biomaterials*, *31*, 7503–7511, 2010.

42. Min, B.-M.; Lee, G.; Kim, S.H.; Nam, Y.S.; Lee, T.S.; Park, W.H. Electrospinning of Silk Fibroin Nanofibers and Its Effect on the Adhesion and Spreading of Normal Human Keratinocytes and Fibroblasts in Vitro. *Biomaterials*, *25*, 1289–1297, 2004.

43. Kim, T.G.; Shin, H.; Lim, D.W. Biomimetic Scaffolds for Tissue Engineering. *Adv Funct Mater*, *22*, 2446–2468, 2012.

44. Huang, Z.-M.; Zhang, Y.-Z.; Kotaki, M.; Ramakrishna, S. A Review on Polymer Nanofibers by Electrospinning and Their Applications in Nanocomposites. *Compos Sci Technol*, *63*, 2223–2253, 2003.

45. Mandal, D.; Shirazi, A.N.; Parang, K. Self-Assembly of Peptides to Nanostructures. *Org Biomol Chem*, *12*, 3544–3561, 2014.

46. Beachley, V.; Wen, X. Polymer Nanofibrous Structures: Fabrication, Biofunctionalization, and Cell Interactions. *Prog Polym Sci*, *35*, 868–892, 2010.

47. Grémare, A.; Guduric, V.; Bareille, R.; Heroguez, V.; Latour, S.; L'heureux, N.; Fricain, J.; Catros, S.; Nihouannen, D.L. Characterization of Printed PLA Scaffolds for Bone Tissue Engineering. *J Biomed Mater Res A*, *106*, 887–894, 2018.

48. Xue, J.; Wu, T.; Dai, Y.; Xia, Y. Electrospinning and Electrospun Nanofibers: Methods, Materials, and Applications. *Chem Rev*, *119*, 5298–5415, 2019.

49. Nemati, S.; Kim, S.; Shin, Y.M.; Shin, H. Current Progress in Application of Polymeric Nanofibers to Tissue Engineering. *Nano Convergence*, *6*, 36, 2019.

50. Sukigara, S.; Gandhi, M.; Ayutsede, J.; Micklus, M.; Ko, F. Regeneration of Bombyx Mori Silk by Electrospinning—Part 1: Processing Parameters and Geometric Properties. *Polymer*, *44*, 5721–5727, 2003.

51. Zhang, X.; Reagan, M.R.; Kaplan, D.L. Electrospun Silk Biomaterial Scaffolds for Regenerative Medicine. *Adv Drug Deliver Rev*, *61*, 988–1006, 2009.

52. Jin, H.-J.; Fridrikh, S.V.; Rutledge, G.C.; Kaplan, D.L. Electrospinning Bombyx Mori Silk with Poly(Ethylene Oxide). *Biomacromolecules*, *3*, 1233–1239, 2002.

53. Jin, H.-J.; Chen, J.; Karageorgiou, V.; Altman, G.H.; Kaplan, D.L. Human Bone Marrow Stromal Cell Responses on Electrospun Silk Fibroin Mats. *Biomaterials*, *25*, 1039–1047, 2004.

54. Wang, H.; Zhang, Y.; Shao, H.; Hu, X. Electrospun Ultra-Fine Silk Fibroin Fibers from Aqueous Solutions. *J Mater Sci*, *40*, 5359–5363, 2005.

55. Kishimoto, Y.; Morikawa, H.; Yamanaka, S.; Tamada, Y. Electrospinning of Silk Fibroin from All Aqueous Solution at Low Concentration. *Materials Science and Engineering: C*, *73*, 498–506, 2017.

56. Nazarov, R.; Jin, H.-J.; Kaplan, D.L. Porous 3-D Scaffolds from Regenerated Silk Fibroin. *Biomacromolecules*, *5*, 718–726, 2004.

57. Kuboyama, N.; Kiba, H.; Arai, K.; Uchida, R.; Tanimoto, Y.; Bhawal, U.K.; Abiko, Y.; Miyamoto, S.; Knight, D.; Asakura, T.; et al. Silk Fibroin - based Scaffolds for Bone Regeneration. *J Biomed Mater Res Part B Appl Biomaterials*, *101B*, 295–302, 2013.

58. Tamada, Y. New Process to Form a Silk Fibroin Porous 3-D Structure. *Biomacromolecules*, *6*, 3100–3106, 2005.

59. Kameda, T.; Hashimoto, T.; Tamada, Y. Effects of Supercooling and Organic Solvent on the Formation of a Silk Sponge with Porous 3-D Structure, and Its Dynamical and Structural Characterization Using Solid-State NMR. *J Mater Sci*, *46*, 7923–7930, 2011.

60. Hirakata, E.; Tomita, N.; Tamada, Y.; Suguro, T.; Nakajima, M.; Kambe, Y.; Yamada, K.; Yamamoto, K.; Kawakami, M.; Otaka, A.; et al. Early Tissue Formation on Whole - area Osteochondral Defect of Rabbit Patella by Covering with Fibroin Sponge. *J Biomed Mater Res Part B Appl Biomaterials*, *104*, 1474–1482, 2016.

61. Ikada, Y. Structure and Properties of Biological Gels. *Kobunshi*, *37*, 742–745, 1988.

62. Ratner, B.D.; Hoffman, A.S. Synthetic Hydrogels for Biomedical Applications. *ACS Symposium Series*, *1*, 1-36, 1976.

63. Huynh, D.P.; Nguyen, M.K.; Pi, B.S.; Kim, M.S.; Chae, S.Y.; Lee, K.C.; Kim, B.S.; Kim, S.W.; Lee, D.S. Functionalized Injectable Hydrogels for Controlled Insulin Delivery. *Biomaterials*, *29*, 2527–2534, 2008.

64. Mo, R.; Jiang, T.; Di, J.; Tai, W.; Gu, Z. Emerging Micro- and Nanotechnology Based Synthetic Approaches for Insulin Delivery. *Chem Soc Rev*, *43*, 3595–3629, 2014.

65. Maity, B.; Samanta, S.; Sarkar, S.; Alam, S.; Govindaraju, T. Injectable Silk Fibroin-Based Hydrogel for Sustained Insulin Delivery in Diabetic Rats. *Acs Appl Bio Mater*, *3*, 3544–3552, 2020.

66. Samal, S.K.; Kaplan, D.L.; Chiellini, E. Ultrasound Sonication Effects on Silk Fibroin Protein. *Macromol Mater Eng*, *298*, 1201–1208, 2013.

67. Yucel, T.; Cebe, P.; Kaplan, D.L. Vortex-Induced Injectable Silk Fibroin Hydrogels. *Biophys J*, *97*, 2044–2050, 2009.

68. Kim, U.-J.; Park, J.; Li, C.; Jin, H.-J.; Valluzzi, R.; Kaplan, D.L. Structure and Properties of Silk Hydrogels. *Biomacromolecules*, *5*, 786–792, 2004.

69. Mallepally, R.R.; Marin, M.A.; McHugh, M.A. CO2-Assisted Synthesis of Silk Fibroin Hydrogels and Aerogels. *Acta Biomater*, *10*, 4419–4424, 2014.

70. Yucel, T.; Kojic, N.; Leisk, G.G.; Lo, T.J.; Kaplan, D.L. Non-Equilibrium Silk Fibroin Adhesives. *J Struct Biol*, *170*, 406–412, 2010.

71. Kasoju, N.; Hawkins, N.; Pop-Georgievski, O.; Kubies, D.; Vollrath, F. Silk Fibroin Gelation via Non-Solvent Induced Phase Separation. *Biomater Sci-uk*, *4*, 460–473, 2016.

72. Hiraide, S. Development of Use Technology of Biomechanical Materials for Medical Products and Life Related Products. *Nagano Prefecture General Industrial Technology Center*, *2*, 136-139, 2007.

73. Ito, T.; Kameda, T.; Tsuji, Y.; Tonooka, N. Suppressing Gelation and Promoting Skin Absorption of Silk Fibroin Aqueous Solution, *J Silk Sci Tech Jpn*, *23*, 57-65, 2015.

74. JP patent, P2015-140328A

75. JP patent, P2005-60404A

76. Hirao, K.; Igarashi, K. シルクフィブロインの特性と食品への利用,

Journal of Cookery Science of Japan, *46*, 54-58, 2013.

77. Nunes, R.W.; Martin, J.R.; Johnson, J.F. Influence of Molecular Weight and Molecular Weight Distribution on Mechanical Properties of Polymers. *Polym Eng Sci*, *22*, 205–228, 1982.

78. Montfort, J.P.; Marin, G.; Monge, P. Molecular Weight Distribution Dependence of the Viscoelastic Properties of Linear Polymers: The Coupling of Reptation and Tube-Renewal Effects. *Macromolecules*, *19*, 1979–1988, 1986.

79. Zhang, J.; Yamagishi, N.; Gotoh, Y.; Potthast, A.; Rosenau, T. High Performance Cellulose Fibers Regenerated from 1 - butyl - 3 - methylimidazolium Chloride Solution: Effects of Viscosity and Molecular Weight. *J Appl Polym Sci*, *137*, 48681, 2020.

80. Michud, A.; Hummel, M.; Sixta, H. Influence of Molar Mass Distribution on the Final Properties of Fibers Regenerated from Cellulose Dissolved in Ionic Liquid by Dry-Jet Wet Spinning. *Polymer*, *75*, 1–9, 2015.

81. Shen, H.; Xie, B.; Yang, W.; Yang, M. Thermal and Rheological Properties of Polyethylene Blends with Bimodal Molecular Weight Distribution. *J Appl Polym Sci*, *129*, 2145–2151, 2013.

82. Tanaka, K.; Takahara, A.; Kajiyama, T. Effect of Polydispersity on Surface Molecular Motion of Polystyrene Films. *Macromolecules*, *30*, 6626–6632, 1997.

83. Kim, J.; Kim, Y.; Kim, C. Effects of Molecular Weight Distribution on the Spinodal Temperature of Polymer Mixtures. *Polym Int*, *53*, 2059–2065, 2004.

84. Xu, S.; Trujillo, F.J.; Xu, J.; Boyer, C.; Corrigan, N. Influence of Molecular Weight Distribution on the Thermoresponsive Transition of Poly(N - isopropylacrylamide). *Macromol Rapid Comm*, 2100212, 2021.

85. Nadgorny, M.; Gentekos, D.T.; Xiao, Z.; Singleton, S.P.; Fors, B.P.; Connal, L.A. Manipulation of Molecular Weight Distribution Shape as a New Strategy to Control Processing Parameters. *Macromol Rapid Comm*, *38*, 1700352, 2017.

86. Shimura, K. Chemical Composition and Biosynthesis of Silk Proteins. *Experientia*, *39*, 455–461, 1983.

87. Inoue, S.; Tanaka, K.; Arisaka, F.; Kimura, S.; Ohtomo, K.; Mizuno, S. Silk Fibroin of Bombyx Mori Is Secreted, Assembling a High Molecular Mass Elementary Unit Consisting of H-Chain, L-Chain, and P25, with a 6:6:1 Molar Ratio*. *J Biol Chem*, *275*, 40517–40528, 2000.

88. Dou, H.; Zuo, B. Effect of Sodium Carbonate Concentrations on the Degumming and Regeneration Process of Silk Fibroin. *J Text Inst*, *106*, 311–319, 2014.

89. Mathur, A.B.; Tonelli, A.; Rathke, T.; Hudson, S. The Dissolution and Characterization of *Bombyx mori* Silk Fibroin in Calcium Nitrate-Methanol Solution and the Regeneration of Films. *Biopolymers*, *42*, 61–74, 1997.

90. Ajisawa, A. STUDIES ON THE DISSOLUTION OF SILK FIBROIN. *Sen'i Gakkaishi*, *24*, 61–64, 1968.

91. Tsukada, M.; Goto, Y.; Minoura, N. Characterization of the regenerated silk fibroin from *Bombyx mori*. *J. Seric. Sci. Jpn.*, *59*, 325–330, 1990.

92. Lee, S.; Kim, S.H.; Jo, Y.; Ju, W.; Kim, H.; Kweon, H. Conformation Transition Kinetics of Silk Fibroin in Aqueous Solution Explored Using Circular Dichroism Spectroscopy. *Chem*, *6*, 1735–1740, 2021.

93. Sha, X.-M.; Tu, Z.-C.; Liu, W.; Wang, H.; Shi, Y.; Huang, T.; Man, Z.-Z. Effect of Ammonium Sulfate Fractional Precipitation on Gel Strength and Characteristics of Gelatin from Bighead Carp (Hypophthalmichthys Nobilis) Scale. *Food Hydrocolloid*, *36*, 173–180, 2014.

94. Hofmeister, F. Zur Lehre von Der Wirkung Der Salze. *Archiv Für Exp Pathologie Und Pharmakologie*, *24*, 247–260, 1888.

95. Kunz, W.; Henle, J.; Ninham, B.W. 'Zur Lehre von Der Wirkung Der Salze' (about the Science of the Effect of Salts): Franz Hofmeister's Historical Papers. *Curr Opin Colloid In*, *9*, 19–37, 2004.

96. Eursakun, S.; Simsiriwong, P.; Ratanabanangkoon, K. Studies on the Fractionation of Equine Antivenom IgG by Combinations of Ammonium Sulfate and Caprylic Acid. *Toxicon*, *60*, 1022–1029, 2012

97. Shimura, K.; Kikuchi, A.; Ohtomo, K.; Katagata, Y.; Hyodo, and A. Studies on Silk Fibroin of Bombyx Mor. *J Biochem*, *80*, 693–702, 1976.

98. Ohmi, S. *Saibou Kougaku shi*; Gakken Medical Shujunsha Co., Ltd.: Tokyo, Japan, 856–861, 1996.

99. Navas, A.A. Use of a Programmable Pocket Calculator for Data Reduction in GPC: Calculation of Molecular Weights and Molecular Weight Distribution. *J Liq Chromatogr*, *5*, 413–423, 2006.

100. Gavin, W. GPC-Gel Permeation Chromatography aka Size Exclusion Chromatography–SEC.

Available online: https://crf.uml.edu/gc.php?u=%2Ffmi%2Fxml%2Fcnt%2Fgpc-Training-2.pdf%3F-db%3DUML_CoreResearchFacilities%26-lay%3DPHP_Resource%26-recid%3D1696%26-field%3Dresource_DOCUMENT%3A%3ADocument%281%29.1639 (accessed on 29 December 2021).

101. DJK Corp.

Available online: https://www.djklab.com/parts/service/pdf/GPC-1.pdf (accessed on 29 December 2021).

102. Tamada, Y.; Ikada, Y. Cell Attachment to Various Polymer Surfaces. In *Polymers in medicine II*. Chiellini, E., Giusti, P., Migliaresi, C., Nicolais, L., Eds.; Springer: Boston, MA, USA, *34*, 101–115, 1986.

103. Schein, C.H. Solubility as a Function of Protein Structure and Solvent Components. *Bio Technology*, *8*, 308–317, 1990.

104. Zhou, C.; Confalonieri, F.; Jacquet, M.; Perasso, R.; Li, Z.; Janin, J. Silk Fibroin: Structural Implications of a Remarkable Amino Acid Sequence. *Proteins Struct Funct Bioinform*, *44*, 119–122, 2001.

105. Marsh, R.E.; Corey, R.B.; Pauling, L. An Investigation of the Structure of Silk Fibroin. *Biochim Biophys Acta*, *16*, 1–34, 1955.

106. Asakura, T.; Kuzuhara, A.; Tabeta, R.; Saito, H. Conformational Characterization of Bombyx Mori Silk Fibroin in the Solid State by High-Frequency Carbon-13 Cross Polarization-Magic Angle Spinning NMR, x-Ray Diffraction, and Infrared Spectroscopy. *Macromolecules*, *18*, 1841–1845, 1985.

107. Saitô, H.; Iwanaga, Y.; Tabeta, R.; Narita, M.; Asakura, T. A High Resolution ^{13}C NMR Study of Silk Fibroin in Solid State by the Cross

Polarization-Magic Angle Spinning Method: Conformational Characterization Utilizing Conformation-Dependent ^{13}C Chemical Shifts. *Chem Lett*, *12*, 427–430, 1983.

108. Zhao, C.; Asakura, T. Structure of Silk Studied with NMR. *Prog Nucl Mag Res Sp*, *39*, 301–352, 2001.

109. Lu, Q.; Hu, X.; Wang, X.; Kluge, J.A.; Lu, S.; Cebe, P.; Kaplan, D.L. Water-Insoluble Silk Films with Silk I Structure. *Acta Biomater*, *6*, 1380–1387, 2010.

110. Tretinnikov, O.N.; Tamada, Y. Influence of Casting Temperature on the Near-Surface Structure and Wettability of Cast Silk Fibroin Films. *Langmuir*, *17*, 7406–7413, 2001.

111. Rockwood, D.N.; Preda, R.C.; Yücel, T.; Wang, X.; Lovett, M.L.; Kaplan, D.L. Materials Fabrication from Bombyx Mori Silk Fibroin. *Nat Protoc*, *6*, 1612–1631, 2011.

112. Vepari, C.; Kaplan, D.L. Silk as a Biomaterial. *Prog Polym Sci*, *32*, 991–1007, 2007.

113. Kundu, B.; Rajkhowa, R.; Kundu, S.C.; Wang, X. Silk Fibroin Biomaterials for Tissue Regenerations. *Adv Drug Deliver Rev*, *65*, 457–470, 2013.

114. Kishimoto, Y.; Morikawa, H.; Yamanaka, S.; Tamada, Y. Electrospinning of Silk Fibroin from All Aqueous Solution at Low Concentration. *Materials Science and Engineering: C*, *73*, 498–506, 2017.

115. Cho, H.J.; Yoo, Y.J.; Kim, J.W.; Park, Y.H.; Bae, D.G.; Um, I.C. Effect of Molecular Weight and Storage Time on the Wet- and Electro-Spinning of Regenerated Silk Fibroin. *Polymer Degradation and Stability*, *97*, 1060–1066, 2012

116. Park, B.K.; Um, I.C. Effect of Molecular Weight on Electro-Spinning Performance of Regenerated Silk. *International Journal of Biological Macromolecules*, *106*, 1166-1172, 2018.

117. Tamada, Y. New Process to Form a Silk Fibroin Porous 3-D Structure. *Biomacromolecules*, *6*, 3100–3106, 2005.

118. Wang, H.; Zhang, Y.; Shao, H.; Hu, X. Electrospun Ultra-Fine Silk Fibroin Fibers from Aqueous Solutions. *J Mater Sci*, *40*, 5359–5363, 2005.

119. Ayub, Z.H.; Arai, M.; Hirabayashi, K. Mechanism of the Gelation of Fibroin Solution. *Biosci Biotechnology Biochem*, *57*, 1910–1912, 1993.

120. Matsumoto, A.; Chen, J.; Collette, A.L.; Kim, U.-J.; Altman, G.H.; Cebe, P.; Kaplan, D.L. Mechanisms of Silk Fibroin Sol−Gel Transitions. *J Phys Chem B*, *110*, 21630–21638, 2006.

121. Li, X.; Yan, S.; Qu, J.; Li, M.; Ye, D.; You, R.; Zhang, Q.; Wang, D. Soft Freezing-Induced Self-Assembly of Silk Fibroin for Tunable Gelation. *Int J Biol Macromol*, *117*, 691–695, 2018.

122. Aznar-Cervantes, S.D.; Lozano-Pérez, A.A.; Montalbán, M.G.; Víllora, G.; Vicente-Cervantes, D.; Cenis, J.L. Importance of Refrigeration Time in the Electrospinning of Silk Fibroin Aqueous Solutions. *J Mater Sci*, *50*, 4879–4887, 2015.

123. Cho, H.J.; Ki, C.S.; Oh, H.; Lee, K.H.; Um, I.C. Molecular Weight Distribution and Solution Properties of Silk Fibroins with Different Dissolution Conditions. *International Journal of Biological Macromolecules*, *51*, 2012.

124. Zainuddin; Le, T.T.; Park, Y.; Chirila, T.V.; Halley, P.J.; Whittaker, A.K. The Behavior of Aged Regenerated Bombyx Mori Silk Fibroin Solutions Studied by 1H NMR and Rheology. *Biomaterials*, *29*, 4268–4274, 2008.

125. Yin, Z.; Wu, F.; Xing, T.; Yadavalli, V.K.; Kundu, S.C.; Lu, S. A Silk Fibroin Hydrogel with Reversible Sol–Gel Transition. *Rsc Adv*, *7*, 24085–24096, 2017.

126. Cho, H. J.; Um, I. C. The Effect of Molecular Weight on the Gelation Behavior of Regenerated Silk Solutions. *Int J Industrial Entomology*, *23*, 183–186, 2011.

127. Aratani, E.; Kameda, T.; Tamada, Y.; Kojima, K. Gelation control of silk fibroin solution during the dialysis process, *J Silk Sci Tech Jpn*, *20*, 85-87, 2013.